Original research article

Physico-chemical characterization and estimation of antimicrobial activity of modified aspirin in the form of nano-organometallic compounds

Abstract:

Aspirin is one of the most commonly used drugs. It is necessary to find and develop safe analgestic anti-inflammatory drugs against their adverse effects. From this standpoint, new nano-organometallic Cu(**II**), Mn(**II**), Ni(**II**), Cd(**II**) and Zn(**II**) compounds of modified aspirin had been prepared and characterized using elemental and spectroscopic techniques such as infrared and ultraviolet, proton nuclear magnetic resonance, mass spectroscopy, electron spin resonance and electron microscope as well as magnetism, conductivity and thermal analyses. The thermal and spectral results showed octahedral geometry and stability of these compounds up to 45^{o}C. The data indicated that, using low concentration against microbes, aspirin and ligand no effect was observed, however, the complexes showed moderate to high effect, The order for Gram positive is Cd(**II**) complex (**10**)> Cd(**II**) complex (**11**)> ampicillin> Zn(**II**) complex (**8**)> Cu(**II**) complex (**4**)> Cu(**II**) complex (**6**)= Ni(**II**) complex (**12**)> Cu(**II**) complex (**2**) = Cu(**II**) complex (**3**)> ligand **(1)**> aspirin> Mn(**II**)complex(**14**) and for Gram negative is ampicillin> Cd(**II**) complex (**10**)> Cd(**II**) complex (**11**)> Cu(**II**) complex (**2**) > Cu(**II**) complex (**6**)> Cu(**II**) complex (**3**)> Cu(**II**) complex (**4**) > Zn(**II**) complex (**8**)> aspirin> Ni(**II**) complex (**12**) > ligand (**1**)> Mn(**II**) complex (**14)** and for *Aspergillus flavus* is Cd(**II**) complex (**10**)>amphotericin B> Cd(**II**) complex (**11**)> ligand (**1**)= aspirin= Cu(**II**) complex (**2**)= Cu(**II**) complex (**3**)= Cu(**II**) complex (**4**)= Cu(**II**) complex (**6**) = Zn(**II**) complex (**8**)= Ni(**II**) complex (**12**)= Mn(**II**) complex (**14**) and for *Candida albicans* is Cd(**II**) complex (**10**) > Cd(**II**) complex (**11**)> amphotericin B > Ni(**II**) complex (**12**)> Cu(**II**) complex (**3**)= Cu(**II**) complex (**6**)> Cu(**II**) complex (**2**)= Cu(**II**) complex (**4**)> ligand**(1)** = aspirin= Zn(**II**) complex (**8**)= Mn(**II**) complex (**14**). The order of catalytic effect of the tested complexes on decomposition of H_2O_2 was Mn(**II**) complex (**14**) > Ni(**II**) complex (**12**) > Cu(**II**) complex (**4**) > Cu(**II**) complex (**6**)> Cu(**II**) complex (**2**) respectively.

Keywords:-

Nano-organometallic compounds, elemental analysis, spectra, magnetism, antimicrobial activity, catalytic activity.

Introduction:-

The chemistry of metal(**II**) carboxylate complexes especially with N-donor ligands has been extensively studied over the last few decades [1, 2]. Some transition metal complexes possess a wide range of

biological activities such as analgesic, anti-inflammatory, antimicrobial, antiviral properties and may serve as antitumor agents, enzyme inhibitors and chemical nucleases [3, 4]. The introduction of metal ions or metal ion binding components into a biological system for the treatment of diseases is one of the main subdivisions in the field of bioinorganic chemistry [5]. Such an intentional introduction of metal ions into the human biological system has proven to be useful for both diagnostic and therapeutic purposes. The role of antibiotic-metal complexes (AMC) in the field of modern pharmacy is constantly expanding. It is necessary to search for new, more effective and more broadly acting drugs [6]. The complexes of antibiotics with metal ions offer great opportunities in this matter. The main reason for that is probably the fact, that many drugs possess modified pharmacological and toxicological properties when they appear in the form of metal complexes [7-11]. Aspirin is a widely used medicine for antipyretic, analgesic, and anti-inflammatory [12]. The demand of aspirin and its derivatives for other biological properties is increasing due to its availability and reactivity as precursor for further modification via corresponding carboxyl group [13]. Aspirin derivatives have shown antibacterial activities against Bacillus subtilis, Escherichia coli, Staphylococcus aureus, and Pseudomonas aeruginosa [14, 15]. Other significant biological properties of aspirin derivatives are reported for antitumor, anticancer, antifungal, and antimicrobial agents [16, 17]. Urea (chemical formula: CH_4N_2O), also known as carbamide, is a polar, hygroscopic molecule [18].The importance of urea in dermatology is twofold: it primarily has a physiological key role for the maintenance of skin hydration, and it secondarily has been used for more than a century in different topical preparation and concentration in various skin conditions. One of the first uses of urea was the topical treatment of wounds because of its antibacterial and proteolytic properties [19].The importance of urea in the treatment of wound healing declined as it was overcome by the development of more specific and effective medications, while its use as moisturiser and keratolytic agent became more popular. Several studies were conducted on the application of urea in the treatment of xerosis, atopic dermatitis, ichthyosis, psoriasis and other conditions, where low concentrations were generally used on the face and body as general emollients, whereas higher concentrations for thickened skin areas or nails or where a fast and keratolytic action was needed [20] Another field of growing interest was the association of urea with other active ingredients, such as topical corticosteroids [21] and antifungals [22] in order to enhance their penetration into the skin. This paper outlines recent topic on preparation and characterization of new nano-organometallic compounds of modified aspirin hopping to find new antimicrobial drugs.

EXPERIMENTAL:

• Materials

The starting chemicals were of analytical grade and used without further purification.

• Physical and spectroscopic techniques

The characterization of the ligand and its metal complexes was carried out using various elemental and spectroscopic techniques such as:- Elemental analyses (C, H, N and Cl) were performed by analytical laboratory of Cairo University, Egypt.

• Molar conductivity:

The molar conductivity of 10^{-3} M of compounds in dimethyl-sulfoxide (DMSO) was determined using Bibby conductimeters MCI at room temperature. Molar conductivities were calculated according to the following equation:

$\Lambda_M = V*K*g/Mw *\Omega$

Where: Λ_M = molar conductivity ($ohm^{-1}cm^2mol^{-1}$) V=volume of the solution (100 cm^3)

K = cell constant: 0.92 cm^{-1}

Mw = molecular weight of the complex

g = grams of complex dissolved in 100 cm^3 solution
Ω = resistance measured in ohms

• **Mass spectra:**

The mass spectra of the compounds were recorded on JEOL JMS-XA- 500 mass spectrometer.

• **Thermal analyses:**

DTA and TGA were carried out on a Shimadzu DT-30 thermal analyzer in nitrogen atmosphere, from room temperature to 600 ℃ at a heating rate of 10 ℃ per minute.

• **^{1}H-NMR spectra:**

The ^{1}H-NMR spectra were recorded on a JEOL EX-270 MHZ FT-NMR spectrometer in deuterated dimethylsulfoxide (DMSO -d^6) as a solvent. The chemical shifts were measured relative to the solvent peaks.

• **IR spectra:**

The infrared spectra of the ligand and its complexes were recorded on Perkin Elmer's infrared spectrometer 681 using KBr or CsBr discs.

• **Electronic absorption spectra:**

The electronic absorption spectra of the compounds were recorded on UNICO SQ-4802 UV/ Vis. Double beam spectrophotometer (190- 1100 nm) using 1 cm quartz cell using DMSO as a solvent.

• **Magnetic susceptibility**

The magnetic susceptibilities of the solid compounds at room temperature were measured in a borosilicate tube with a Johnson Matthey at room temperature using the following equations:

$Xa = [2.086\ L\ (R- R^o) / (109W)]$

$Xm = X_a * Mw$

$Xn = X_m – D$

$\mu_{eff} = 2.828\ (X_n \times T)^{1/2}$ Where:-

Xa = mass susceptibility L = sample length in cm

R = tube + sample reading R^o = empty the reading

W = mass of the sample Xm = molar susceptibility Mw = molecular weight

Xn = corrected molar susceptibility D = diamagnetic corrections

μ_{eff} = effective magnetic moment T = room temperature in Kelvin.

• **Transmission electron microscopy characterization (TEM)**

TEM samples for colloidal suspension of Cd(II) complex(**10**) in distilled water were prepared by dropping the colloids onto carbon-coated TEM grids and allowing the liquid carrier to evaporate in air then assayed by a JEOL JEM-1230 Electron Microscope.

• **Determination of metal content**

Metal content was determined using colorimetric method on HACH DR 5000 spectrophotometer [23-25].

• **ESR spectra**

The solid ESR spectra of some complexes were recorded at room temperature using ELEXSYS E500 Bruker spectrometer in 3 nm Pyrex Tubes at 25℃. Diphenylpicrl-hydrazide (DPPH) free radical was used as a g- maker for the calibration of the spectra. The equation used to determine g- values was

$g = (g_{DPPH})\ (H_{DPPH}) / H$ Where: $g_{DPPH} = 2.0036$

H_{DPPH} = magnetic field of DPPH in gauss H = magnetic field of the sample in gauss.

• **Preparation of the ligand (1) :**

It was prepared by refluxing with stirring two hours of (2-acetoxy-5-sulfobenzoic acid) (30.00 g, 3.597 mol) dissolved in 30 cm^3 ethanol with (urea) (6.08 ml, 3.374 mol). The product which formed left to cool at room temperature to give the final ligand (2-acetoxy-5-carbamoylbenzoic acid). Preparation of the ligand (**1**) is shown in **Scheme 1**.

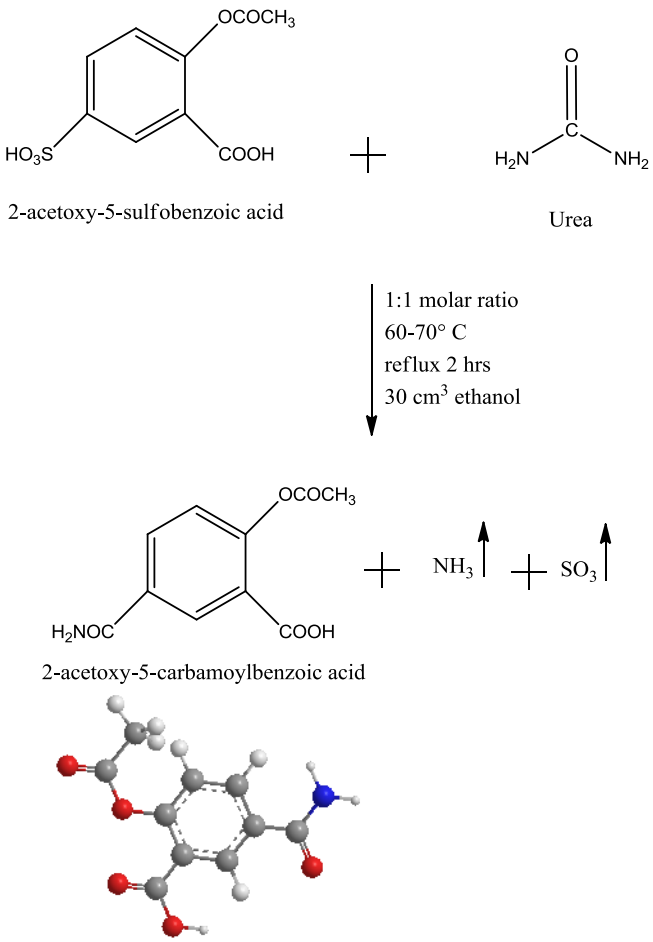

Scheme (1): Preparation of the ligand (1)

Ligand (**1**): Yield 97%; m.p. 150 ; color is pink ; Anal. Calcd. for $C_9H_{10}O_8S$ (FW=223): C, 53.50; H, 4.00; N, 6.20. Found (%) C, 53.81; H, 4.04; N, 6.28, IR (KBr, cm^{-1}), 3413 υ(OH), 1616 υ($CONH_2$), 1660 υ(C=O) acetyl, 1704 υ(C=O) carboxylic; The mass spectrum of the ligand (1) revealed molecular ion peak at m/z 223. Analytical data for ligand (**1**) and its complexes are given in Table (1):-

- **Preparation of metal complexes (2)-(15) :**

The metal complexes (**2-15**) were prepared by refluxing with stirring a suitable amount of a hot ethanolic solution of the following metal salts: $Cu(OAc)_2 . 3H_2O$ (1.60 g, 0.108 mol) complex (**2**), $Cu(OAc)_2 . H_2O$ (0.80 g, 0.039 mol) complex (**3**), $CuSO_4 . 5H_2O$ (1.12 g, 0.076 mol) complex (**4**), $CuSO_4 . 5H_2O$ (0.56 g, 0.028 mol) complex (**5**), $CuCl_2 . 2H_2O$ (1.20 g, 0.089 mol) complex (**6**), $CuCl_2 . 2H_2O$ (0.60 g, 0.003 mol) complex (**7**), $Zn(OAc)_2 . 3H_2O$ (1.97 g, 0.132 mol) complex (**8**), $Zn(OAc)_2 \cdot 3H_2O$ (0.98 g, 0.048 mol) complex(**9**), $Cd(OAc)_2 \cdot 3H_2O$ (2.39 g, 0.147 mol) complex(**10**), $Cd(OAc)_2 . 3H_2O$ (1.20 g, 0.055 mol) complex(**11**), $Ni(OAc)_2 . 4H_2O$ (2.23 g, 0.152 mol) complex(**12**), $Ni(OAc)_2 . 4H_2O$ (1.12 g, 0.055 mol) complex(**13**), $Mn(OAc)_2 . 4H_2O$ (2.20 g, 0.151 mol) complex(**14**), $Mn(OAc)_2 . 4H_2O$ (1.10g, 0.055 mol) complex(**15**) with a hot ethanolic solution of the ligand (**1**) (1.50 ml, 0.2242 mol). The ligand and metal ions used with molar ratios equal to 1L: 1M and 2L: 1M in 30 cm^3 ethanol for 1-3 hrs range. The precipitates which formed were filtered off, washed with ethanol then by diethyl ether and dried in vacuum desiccators over P_4O_{10}.

- **Biological activity**
- **Antimicrobial activity (invitro study):**

Antimicrobial activity of the tested compounds was assessed against Gram positive bacteria (*Staphylococcus aureus*), Gram negative bacteria (*Escherichia coli*) and Fungi (*Aspergillus flavus)* and *(Candida albicans*) using disc diffusion method [26]. Ampicillin was used as a positive control for bacteria and Amphotericin B for fungi and solvent control (DMSO) was also used to know the activity of the solvent. The test compounds were dissolved in DMSO to give concentrations 250, 200, 175, 150 and 125 ppm and a DMSO poured disc was used as negative control. The bacteria were subcultured in nutrient agar medium, which was prepared using peptone, beef extract, NaCl, agar and distilled water. The Petri dishes were incubated for 48 hrs at 37℃. The standard antimicrobial drugs were also screened under similar conditions for comparison. The zone of inhibition was measured in millimeters carefully. All determination was made in duplicate for each of the compounds. An average of the two independent readings for each compound was recorded.

- **Invivo studies (Toxicity study):**

Toxicity study of cadmium(II)complex **(10)** with molecular weight equal to 543 and chemical formula $C_{14}H_{25}O_{14}CdN$ was done. The complex was dissolved in DMSO diluted by sterile saline 0.9 % NaCl in a maximum concentration of 0.2% by volume in order to be able to injected intra peritoneal.

Animals:

Twenty healthy male albino rats 8 weeks old (180 - 200 g) were purchased from National Cancer Institute, Cairo, Egypt. Rats were housed in cages at regulated temperature (22- 25 ℃). They were kept under good ventilation under a photoperiod of 12hr light/12hr darkness schedule with lights-on from 06:00 to 18:00. They all received a standard laboratory diet (60% ground corn meal, 10% bran, 15% ground beans, 10% corn oil, 3% casein, 1% mineral mixture and 1% vitamins mixture), purchased from Meladco Feed Company (Obour City, Cairo, Egypt) and supplied with water ad libitum throughout the experimental period.

Experimental design:

Twenty animals were allowed 10 days for adaptation. They were then randomly distributed into 2 equal groups, 10 rats each. The animal groups were recognized as follows:

Group 1 (Control): Normal healthy control animals.

Group 2: Each animal was injected intra peritoneal with 1x10-5mmole/L of Cd(II) complex (10) for 6weeks.

Blood collection

At the end of the experimental period (6 weeks), blood samples were collected from overnight rats, centrifuged at 3000 rpm for 10 min and the separated sera were frozen at -20 ℃ for future biochemical analysis.

Biochemical analyses

Liver enzymes activities, aspartate aminotransferase (AST) and alanine aminotransferase (ALT) were estimated using kinetic kits purchased by Human Diagnostic Kits, Germany [27]. The liver function, albumin concentration and kidney functions, blood urea and serum creatinine were measured using Diamond Diagnostic kits, Egypt. All biochemical analysis were determined using a Biosystems BTS-310 Spectrophotometer [28].

Hematological analyses

An automated hemogram was done in all cases.This included hemoglobin estimation, red cell count, white blood cells, and platelet count.

These parameters were obtained electronically by colter counter model Beckman 750 Int, U.S.A.

Statistical analysis

Data were subjected to statistical significance tests using one-way analysis of variance (ANOVA), followed by Duncan's multiple range test. The statistical analysis was carried out using SPSS 16.00

software. The results were expressed as mean ± SE and the differences were considered significant at $P \leq 0.05$ [29].

Results and discussion:

The ligand (**1**) and its metal complexes (**2)-(15**) are stable at room temperature, non-hydroscopic and are insoluble in common solvents such as ethanol, acetone, water and chloroform but soluble in DMF and DMSO. The elemental analysis confirmed that, all complexes are composed of the ligand and metal ions with molar ratios equal to 1L: 1M, and 2L: 1M. Many attempts were made to grow a single crystal, but unfortunately, they failed until now. Some of the metal complexes are found in nano form having size range from (5.65 – 11.50 nm) make different properties of these complexes. The analytical, physical and spectral data are presented in experimental part, and Tables (**1**)-(**6**) which are compatible with the suggested structures as shown in figure (**1**).

Table 1:- Analytical and Physical Data of the Ligand (1) and its Metal Complexes.

No.	Ligand/Complexes	Color	FW	M.P (^{O}C)	Yield (%)	Anal. /Found (Calc.) (%)				
						C	**H**	**N**	**M**	**Conductivity Λ**
(1)	**[HL] $C_{10}H_9O_5$ N**	**Off white**	**223**	150	**97**	**53.50 (53.81)**	**4.00 (4.04)**	**6.20 (6.28)**	-	-
(2)	**[(HL)Cu $(OAc)_2(H_2O)_2$].3H_2O $C_{14}H_{25}$ O_{14} Cu N**	**Olive green**	**494**	310	**95**	**33.80 (33.97)**	**5.20 (5.06)**	**2.75 (2.83)**	**12.75 (12.84)**	11.50
(3)	**[$(HL)_2$Cu$(OAc)_2$] .3H_2O $C_{24}H_{30}O_{17}$ Cu N_2**	**Olive green**	**681**	312	**93**	**33.30 (33.46)**	**4.45 (4.40)**	**4.00 (4.11)**	**9.20 (9.32)**	11.00
(4)	**[(HL)Cu $(H_2O)_4$]. SO_4.2H_2O $C_{10}H_{21}$ O_{15} Cu S N**	**Blue**	**490**	315	**90**	**24.40 (24.46)**	**4.65 (4.28)**	**2.70 (2.85)**	**12.60 (12.95)**	103
(5)	**[$(HL)_2$Cu $(SO_4)(H_2O)$].3H_2O $C_{20}H_{26}O_{18}$ Cu S N_2**	**Sky blue**	**677**	320	**92**	**35.30 (35.42)**	**3.70 (3.84)**	**4.05 (4.13)**	**9.35 (9.37)**	13.2
(6)	**[(HL)Cu $(Cl)_2(H_2O)_2$].3H_2O $C_{10}H_{19}O_{10}$ $CuCl_2$N**	**Dark green**	**447**	322	**85**	**26.20 (26.82)**	**4.70 (4.25)**	**3.23 (3.13)**	**15.50 (15.87)**	12.60
(7)	**[$(HL)_2$Cu $(Cl)_2$].3H_2O $C_{20}H_{24}O_{13}$ Cu Cl_2 N_2**	**Light green**	**634**	325	**87**	**37.35 (37.83)**	**3.50 (3.78)**	**4.30 (4.41)**	**10.15 (10.01)**	13.00
(8)	**[(HL)Zn $(OAc)_2(H_2O)_2$].3H_2O $C_{14}H_{25}$ O_{14} Zn N**	**Simon**	**496**	333	**90**	**33.45 (33.85)**	**5.35 (5.04)**	**2.70 (2.82)**	**13.40 (13.16)**	13.50
(9)	**[$(HL)_2$Zn$(OAc)_2$] .3H_2O $C_{24}H_{30}O_{17}$ Zn N_2**	**Pink**	**683**	335	**86**	**42.77 (42.15)**	**4.57 (4.39)**	**4.25 (4.10)**	**9.50 (9.56)**	13.80
(10)	**[(HL)Cd $(OAc)_2(H_2O)_2$].3H_2O $C_{14}H_{25}$ O_{14} Cd N**	**Simon**	**543**	314	**84**	**30.99 (30.94)**	**4.69 (4.60)**	**2.40 (2.58)**	**20.45 (20.70)**	13.00
(11)	**[$(HL)_2$Cd$(OAc)_2$] .3H_2O $C_{24}H_{30}O_{17}$Cd N_2**	**Pink**	**730**	313	**80**	**39.28 (39.43)**	**4.61 (4.11)**	**3.66 (3.83)**	**15.51 (15.39)**	13.20
(12)	**[(HL)Ni $(OAc)_2(H_2O)_2$].3H_2O $C_{14}H_{25}$ O_{14} Ni N**	**Olive green**	**489**	338	**81**	**34.35 (34.31)**	**5.71 (5.11)**	**2.65 (2.86)**	**11.56 (11.97)**	14.00
(13)	**[$(HL)_2$Ni$(OAc)_2$] .3H_2O $C_{24}H_{30}O_{17}$ Ni N_2**	**Grey**	**676**	340	**83**	**33.98 (33.70)**	**4.52 (4.43)**	**4.00 (4.14)**	**8.45 (8.66)**	14.60
(14)	**[(HL)Mn $(OAc)_2(H_2O)_2$].3H_2O $C_{14}H_{25}$ O_{14}Mn N**	**Off white**	**485**	328	**94**	**34.86 (34.58)**	**5.68 (5.15)**	**2.54 (2.88)**	**11.43 (11.30)**	14.50
(15)	**[$(HL)_2$Mn$(OAc)_2$] .3H_2O $C_{24}H_{30}O_{17}$ Mn N_2**	**Beige**	**673**	330	**95**	**42.55 (42.80)**	**4.60 (4.46)**	**4.32 (4.16)**	**8.20 (8.16)**	15.00

*** m^{-1} cm^2 mol^{-1}**

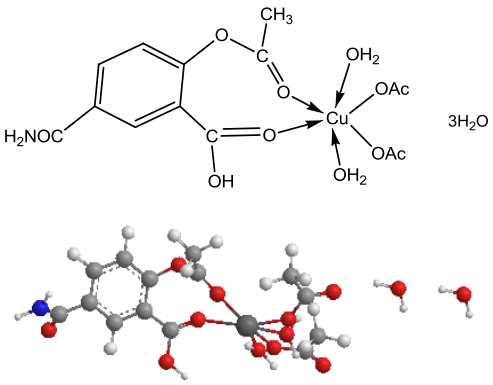

Complex (2)

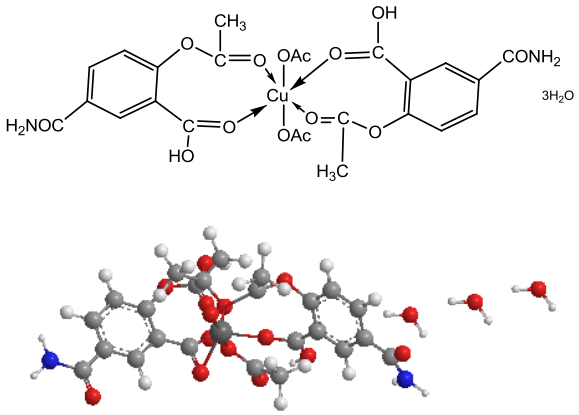

Complex (3)

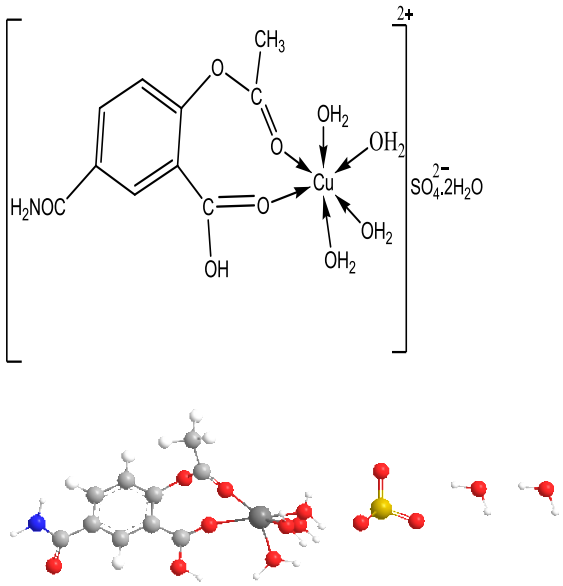

Complex (4)

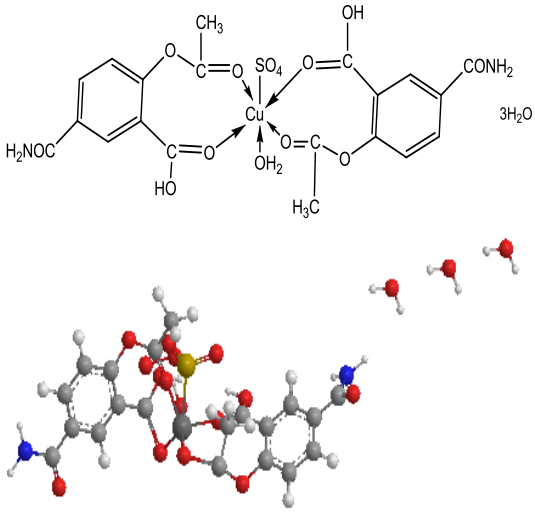

Complex (5)

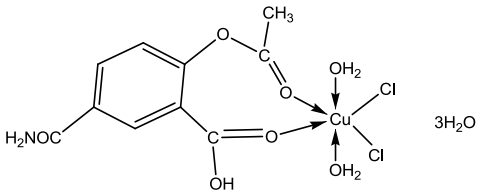

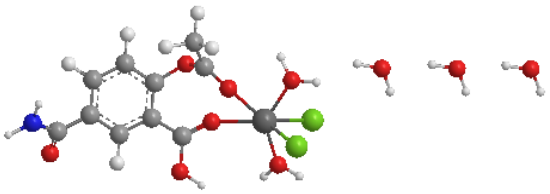

Complex (6)

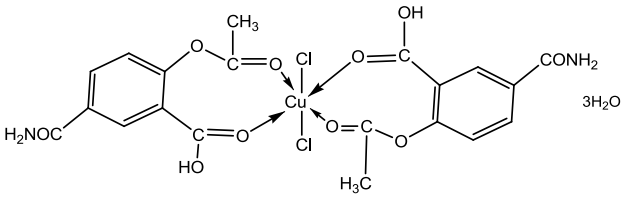

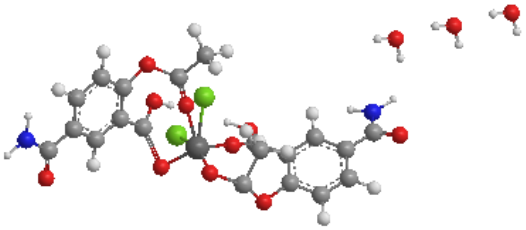

Complex (7)

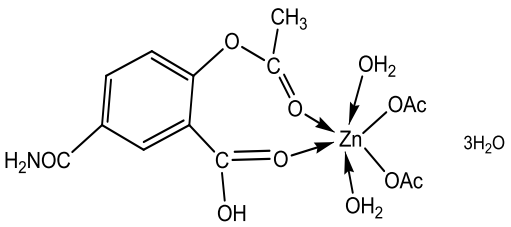

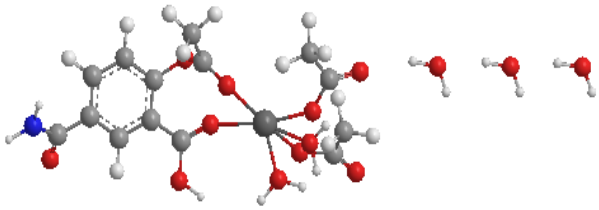

Complex (8)

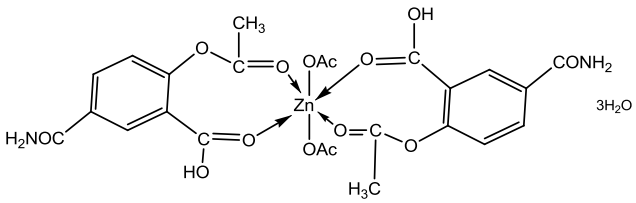

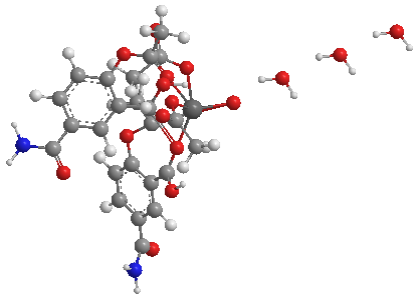

Complex (9)

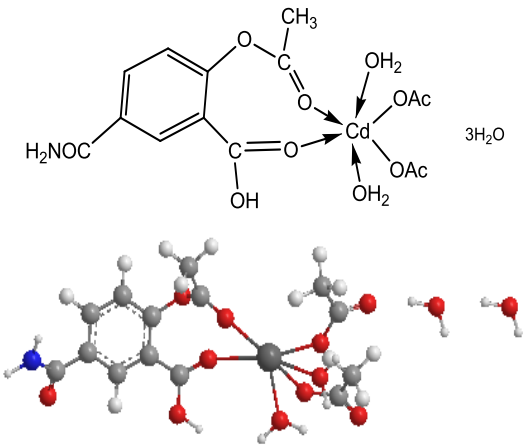

Complex (10)

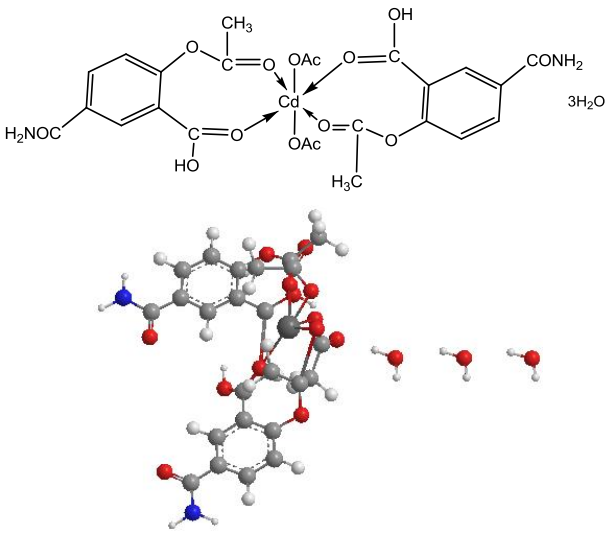

Complex (11)

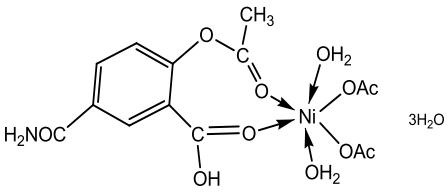

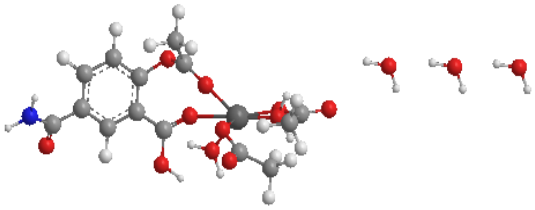

Complex (12)

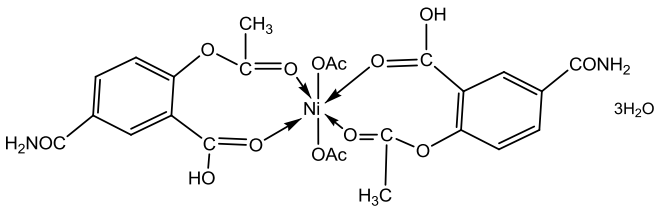

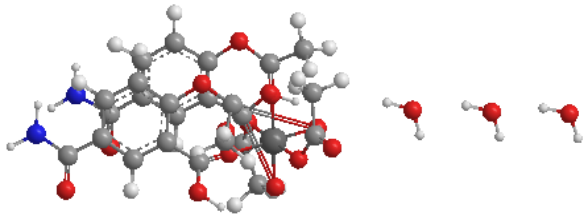

Complex (13)

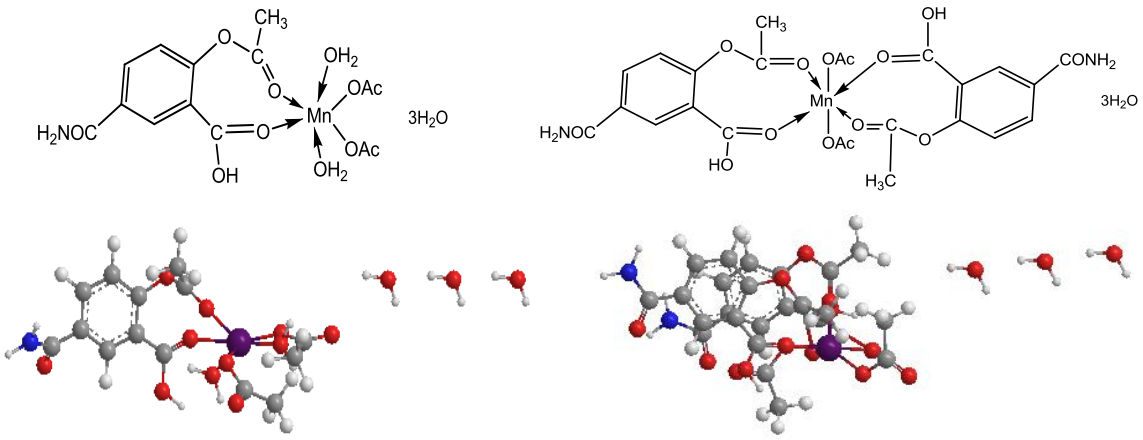

Complex (14) **Complex (15)**

Figure (1): Suggested structures of the ligand (1) and its metal complexes

Transmission electron microscopy characterization (TEM)

TEM images for the colloidal suspensions of Cd(II) complex (10) was obtained. The average diameter of these spherical Cd(II) complex (10) was found to be (5.65 – 11.50) nm as shown in Figure (**2**).

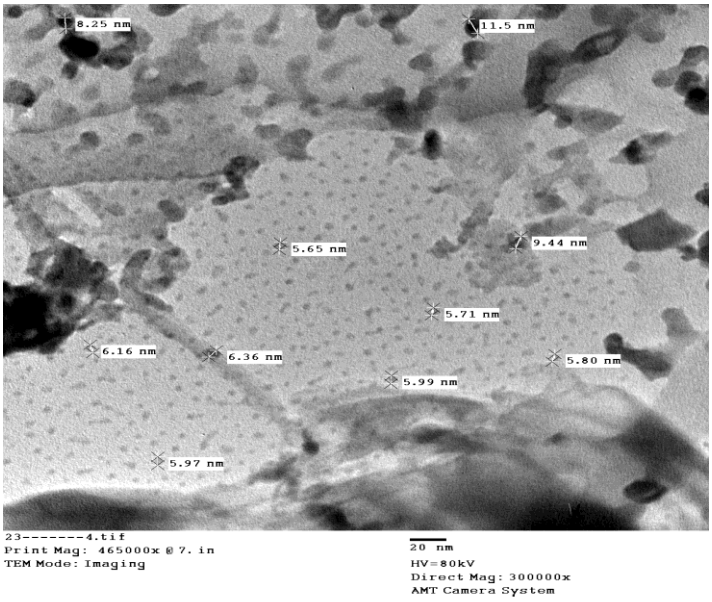

Figure (**2**): Electromicroscopic diagram of complex (**10**)

- **The Molar Conductivity**

The molar conductivities of 1×10^{-3} M solutions of the complexes in DMSO at room temperature were found in the range (11.00- 15.00) ohm^{-1} cm^2 mol^{-1} indicating the non-electrolytic in nature of all complexes except complex (**4**) the value is 103 ohm^{-1} cm^2 mol^{-1},confirming electrolytic nature. These low values commensurate the coordination of the anions to the metal ions [30].

Mass Spectra of the Ligand [HL] and some of its metal complexes:

The mass spectrum of ligand **(1)** [**HL**], (**Table (2,a)**) showed the molecular ion peak at *m/*z 223 amu, confirming its formula weight (F.W. 223).The mass fragmentation patterns observed at *m/z* = 53, 79, 119, 149, 183 and 223 amu correspond to C_3HO, C_5H_3O, C_8H_7O, $C_8H_7O_2N$, $C_8H_9O_4N$ and $C_{10}H_9O_5N$ moieties, respectively, supported the suggested structure of the ligand.

Table (2,a): Mass spectrum of the ligand (1):

Ligand (1)	m/z	Rel. Int.	Fragment
	53	27	C_3HO
	79	32	C_5H_3O
	119	23	C_8H_7O
	149	22	$C_8H_7O_2N$
	183	21	$C_8H_9O_4N$
	223	15	$C_{10}H_9O_5N$

The mass spectrum of **complex (2) (Table (2,b))** showed the molecular ion peak at *m/*z 494 amu, confirming its formula weight (F.W. 494).The mass fragmentation patterns observed at *m/z* = 55, 57, 71, 85, 149, 197, 249, 318, 398, 414, 465 and 494 amu correspond to C_3H_3O, C_5H_5O, C_4H_7O, C_5H_9O, $C_5H_{10}OCu$, $C_5H_{10}O_4Cu$, $C_8H_{10}O_5Cu$, $C_8H_{15}O_9Cu$, $C_8H_{15}O_{14}Cu$, $C_8H_{17}O_{14}NCu$, $C_{12}H_{20}O_{14}NCu$ and $C_{14}H_{25}O_{14}NCu$ moieties, respectively, supported the suggested structure of the complex.

Table (2,b): Mass spectrum of the Cu(II) complex (2):

Complex	m/z	Rel. Int.	Fragment
(2)	55	83	C_3H_3O
	57	100	C_5H_5O
	71	55	C_4H_7O
	85	34	C_5H_9O
	149	35	$C_5H_{10}OCu$
	197	41	$C_5H_{10}O_4Cu$
	249	51	$C_8H_{10}O_5Cu$
	318	23	$C_8H_{15}O_9Cu$
	398	24	$C_8H_{15}O_{14}Cu$
	414	21	$C_8H_{17}O_{14}NCu$
	465	31	$C_{12}H_{20}O_{14}NCu$
	494	17	$C_{14}H_{25}O_{14}NCu$

The mass spectrum of **complex (3) (Table (2,c))** showed the molecular ion peak at *m/*z 681 amu, confirming its formula weight (F.W. 681).The mass fragmentation patterns observed at *m/z* = 55, 71, 97, 149, 199, 293, 387, 465, 544, 625 and 681 amu correspond to C_3H_3O, $C_3H_3O_2$, $C_5H_5O_2$, $C_8H_7O_2N$, $C_{11}H_7O_2N_2$, $C_{12}H_9O_7N_2$, $C_{14}H_{16}O_7N_2Cu$, $C_{15}H_{18}O_{11}N_2Cu$, $C_{16}H_{21}O_{15}N_2Cu$, $C_{20}H_{22}O_{17}N_2Cu$ and $C_{24}H_{30}O_{17}N_2Cu$ moieties, respectively, supported the suggested structure of the complex.

Table (2,c): Mass spectrum of the Cu(**II**) **complex (3):**

Complex	m/z	Rel. Int.	Fragment
(3)	55	44	C_3H_3O
	71	22	$C_3H_3O_2$
	97	22	$C_5H_5O_2$
	149	28	$C_8H_7O_2N$
	199	21	$C_{11}H_7O_2N_2$
	293	100	$C_{12}H_9O_7N_2$
	387	21	$C_{14}H_{16}O_7N_2Cu$
	465	41	$C_{15}H_{18}O_{11}N_2Cu$
	544	51	$C_{16}H_{21}O_{15}N_2Cu$
	625	19	$C_{20}H_{22}O_{17}N_2Cu$
	681	15	$C_{24}H_{30}O_{17}N_2Cu$

The mass spectrum of **complex (8) (Table (2,d))** showed the molecular ion peak at *m/*z 496 amu, confirming its formula weight (F.W. 496).The mass fragmentation patterns observed at *m/z* = 55, 71, 85, 98, 129, 149, 205, 295, 356, 412, 467 and 496 amu correspond to C_3H_3O, $C_3H_3O_2$, $C_4H_5O_2$, $C_5H_6O_2$, $C_5H_7O_3N$, $C_5H_{11}O_4N$, $C_7H_{11}O_6N$, $C_9H_{12}O_6NZn$, $C_{10}H_{13}O_9NZn$, $C_{12}H_{13}O_{11}NZn$, $C_{12}H_{20}O_{14}NZn$ and $C_{14}H_{25}O_{14}NZn$ moieties, respectively, supported the suggested structure of the complex.

Table (2,d): Mass spectrum of the Zn(II) complex (8):

Complex	m/z	Rel. Int.	Fragment
(8)	55	33	C_3H_3O
	71	29	$C_5H_3O_2$
	85	20	$C_4H_5O_2$
	98	51	$C_5H_6O_2$
	129	100	$C_5H_7O_3N$
	149	61	$C_5H_{11}O_4N$
	205	41	$C_7H_{11}O_6N$
	295	45	$C_9H_{12}O_6NZn$
	356	31	$C_{10}H_{13}O_9NZn$
	412	22	$C_{12}H_{13}O_{11}NZn$
	467	21	$C_{12}H_{20}O_{14}NZn$
	496	17	$C_{14}H_{25}O_{14}NZn$

The mass spectrum of **complex (11) (Table (2,e))** showed the molecular ion peak at *m/*z 730 amu, confirming its formula weight (F.W. 730).The mass fragmentation patterns observed at *m/z* = 55, 70, 86, 98, 129, 143, 200, 316, 401, 505, 609, 674 and 730 amu correspond to C_3H_3O, C_3H_4ON, $C_3H_4O_2N$, $C_4H_4O_2N$, $C_4H_5O_3N_2$, $C_5H_7O_3N_2$, $C_7H_8O_5N_2$, $C_7H_{12}O_5N_2Cd$, $C_7H_{17}O_{10}N_2Cd$, $C_{14}H_{21}O_{11}N_2Cd$, $C_{21}H_{25}O_{12}N_2Cd$, $C_{21}H_{26}O_{16}N_2Cd$ and $C_{24}H_{30}O_{17}N_2Cd$ moieties, respectively, supported the suggested structure of the complex.

Table (2,e): Mass spectrum of the Cd(II) complex (11):

Complex	m/z	Rel. Int.	Fragment
(11)	55	77	C_3H_3O
	70	49	C_3H_4ON
	86	31	$C_3H_4O_2N$
	98	26	$C_4H_4O_2N$
	129	100	$C_4H_5O_3N_2$
	143	19	$C_5H_7O_3N_2$
	200	16	$C_7H_8O_5N_2$
	316	51	$C_7H_{12}O_5N_2Cd$
	401	25	$C_7H_{17}O_{10}N_2Cd$
	505	41	$C_{14}H_{21}O_{11}N_2Cd$
	609	23	$C_{21}H_{25}O_{12}N_2Cd$
	674	22	$C_{21}H_{26}O_{16}N_2Cd$
	730	21	$C_{24}H_{30}O_{17}N_2Cd$

The mass spectrum of **complex (13) (Table (2,f))** showed the molecular ion peak at *m/*z 676 amu, confirming its formula weight (F.W. 676).The mass fragmentation patterns observed at *m/z* = 55, 71, 85, 98, 129, 149, 199, 293, 391, 454, 529, 613 and 676 amu correspond to C_3H_3O, $C_3H_3O_2$, $C_3H_3O_2N$, $C_4H_4O_2N$, $C_4H_5O_3N_2$, $C_4H_9O_4N_2$, $C_8H_{11}O_4N_2$, $C_9H_{13}O_9N_2$, $C_{11}H_{13}O_{10}N_2Ni$, $C_{12}H_{16}O_{13}N_2Ni$, $C_{18}H_{19}O_{13}N_2Ni$, $C_{21}H_{19}O_{16}N_2Ni$ and $C_{24}H_{30}O_{17}N_2Ni$ moieties, respectively, supported the suggested structure of the complex.

Table (2,f): Mass spectrum of the Ni(II) complex (13):

Complex	m/z	Rel. Int.	Fragment
(13)	55	53	C_3H_3O
	71	28	$C_3H_3O_2$
	85	28	$C_3H_3O_2N$
	98	91	$C_4H_4O_2N$
	129	25	$C_4H_5O_3N_2$
	149	21	$C_4H_9O_4N_2$
	199	100	$C_8H_{11}O_4N_2$
	293	81	$C_9H_{13}O_9N_2$
	391	29	$C_{11}H_{13}O_{10}N_2Ni$
	454	27	$C_{12}H_{16}O_{13}N_2Ni$
	529	51	$C_{18}H_{19}O_{13}N_2Ni$
	613	24	$C_{21}H_{19}O_{16}N_2Ni$
	676	17	$C_{24}H_{30}O_{17}N_2Ni$

The mass spectrum of **complex (15) (Table (2,g))** showed the molecular ion peak at *m/*z 673 amu, confirming its formula weight (F.W. 673).The mass fragmentation patterns observed at *m/z* = 55, 80, 98, 129, 149, 167, 200, 232, 293, 375, 480, 584 and 673 amu correspond to C_3H_3O, C_5H_4O, $C_5H_6O_2$, $C_5H_7O_3N$, $C_5H_{11}O_4N$, $C_5H_{13}O_5N$, $C_5H_{14}O_7N$, $C_5H_{14}O_9N$, $C_{10}H_{15}O_9N$, $C_{10}H_{19}O_{13}N_2$, $C_{14}H_{21}O_{13}N_2Mn$, $C_{17}H_{25}O_{17}N_2Mn$ and $C_{24}H_{30}O_{17}N_2Mn$ moieties, respectively, supported the suggested structure of the complex.

Table (2,g): Mass spectrum of the Mn(II) complex (15):

Complex	m/z	Rel. Int.	Fragment
(15)	55	100	C_3H_3O
	80	90	C_5H_4O
	98	25	$C_5H_6O_2$
	129	27	$C_5H_7O_3N$
	149	32	$C_5H_{11}O_4N$
	167	51	$C_5H_{13}O_5N$
	200	31	$C_5H_{14}O_7N$
	232	29	$C_5H_{14}O_9N$
	293	31	$C_{10}H_{15}O_9N$
	375	21	$C_{10}H_{19}O_{13}N_2$
	480	23	$C_{14}H_{21}O_{13}N_2Mn$
	584	22	$C_{17}H_{25}O_{17}N_2Mn$
	673	23	$C_{24}H_{30}O_{17}N_2Mn$

- **IR Spectra**

The IR data of the ligand and its metal complexes are shown in Table (**3**). The IR spectra of the ligand (**1**) showed a strong vibration band located at 1680 cm^{-1} which assigned to the carbonyl ν(C=O) of the acetyl group, whereas the broad band which observed at 3413 cm^{-1} is assigned to the stretching vibration of the aromatic hydroxyl group and the other band at 1616 cm^{-1} is assigned to the stretching vibration of the ν($CONH_2$) group. The broad bands appeared at 3560-3230 and 3220-2460 cm^{-1} ranges are assigned to inter- and intramolecular hydrogen bondings [31].These observations confirmed the presence of the ligand in the ketonic form in the solid state [32]. The spectrum of the ligand also showed band at 1740 which may be assigned to ν(C=O) of carboxylic group [33]. The bands appeared at 1421 and 772 cm^{-1}, were assigned to υ(Ar) vibration. By comparing the IR spectral data of the complexes with that of the free ligand. It is noted that, in all complexes the appearance of a new band in the range of 1710-1669 cm^{-1} which may be assigned to the C=O of carboxylic group and this band shifted to lower value confirming coordination of this group to the metal ion [34]. In the spectra of all complexes, the absorption frequency of ν(C=O) of acetyl group was shifted to lower frequency side and appeared in the region 1684-1623 cm^{-1} range with lowering its intensity confirmed the coordination of oxygen atom ν(C=O) of acetyl

group with the metal ions without undergoing enolization. Also, it was observed that, the presence of absorption band due to hydroxyl group which appeared in the spectra of complexes at (3460-3412) cm^{-1} range indicated that, this group is not coordinated to the metal ion Table(**3**) [35]. The appearance of new bands appeared in the 623-588, and 590-541 cm^{-1} ranges for different complexes may be assigned to the ν(M–O) [36]. These results confirmed that, the bonding of the ligand with the metal ions occurred via carbonyl oxygen of acetyl and carboxylic groups [37]. Strong bands appeared at 3370 and 3210 cm^{-1} related to υ(NH_2) respectively. The bands appeared at 1578 and 1565 cm^{-1},were assigned to υ(NH) vibration. The aromatic ring vibrations appeared in the (1482-1434) and (786-770) cm^{-1} ranges. In the case of acetate complexes (**2,3**), (**8-15**) there are two new bands appeared in the 1473-1380 and 1348-1333 cm^{-1} ranges which are attributed to the symmetric and asymmetric stretching vibration of the acetate group. The separation values (Δ) between $\nu_{asym}(COO^-)$ and $\nu_{sym.}(COO^-)$ in these complexes suggesting the coordination of acetate group in as a monodentate fashion [38]. In the case of sulfate complexes there are new bands appeared at 1216, 1175, 1031, 664 for complex (**4**) and 1218, 1158, 1083, 664 for complex (**5**). These bands indicated that, the sulfate ion is coordinated to the metal ion. In the case of chloride complexes (**6**) and (**7**) there are new bands appeared at 445 and 442 cm^{-1} respectively suggesting the coordination of chloride group to metal ion. The appearance of broad bands in the range (1640-1610) cm^{-1} is assigned to the stretching vibrations of the ν($CONH_2$) group. The appearance of broad bands in the ranges (3580-3210) and (3320-3080) cm^{-1} are due to hydrated or coordinated water molecules [39]. However, the hydrogen bondings appeared at (3650-3220) and (3330-2445) cm^{-1} ranges. The above results together with elemental analyses indicated that, the ligand behaved as neutral bidentate fashion bonded to the metal ions through carbonyl oxygen atoms of acetyl and carboxylic groups.

Table (3):- IR frequencies of the bands (cm^{-1}) of the ligand (1) and its metal complexes:

No.	$\nu(H_2O)$	ν(OH)	υ(H-bonding)	ν(C=O) Acetyl	ν(C=O) carb	$\nu(CONH_2)$	$\nu(NH_2)$	ν(C-O)	ν(C-N)	ν(NH)	ν(ON)	ν(Ar)	$\nu(OAc)/SO_4$)	υ(M-O)	υ(M-Cl)
(1)	-	3413	(3560-3230) , (3220-2460)	1660	1704	1616	3250, 3217	1128, 1080	1480	1570	-	(1421, 772)	-	-	-
(2)	(3550-3310) , (3300-3150)	3434	(3550-3260) , (3250-2720)	1635	1675	1615	3255, 3225	1123, 1032	1477	1571	1512	(1440, 770)	1380, 1335	610, 590	-
(3)	(3520-3310), (3300-3150)	3460	(3560-3250), (3240-2870)	1630, 1625	1670, 1655	1613	3300, 3265	1129, 1031	1473	1569	1509	(1445, 773)	1473,1341	604, 541	-
(4)	(3530-3220) , (3210-3135)	3412	(3600-3220), (3210-2560)	1682	1710	1616	3350, 3235	1144, 1089	1585	1572	1530	(1478, 773)	1216, 1175, 1031, 664	623, 589	-
(5)	(3530-3210) , (3200-3125)	3415	(3620-3220) , (3210-2465)	1650	1700, 1684	1618	3370, 3235	1129, 1031	1581	1568	1511	(1480, 773)	1218, 1158, 1083, 664	590, 575	-
(6)	(3530-3330) , (3320-3140)	3424	(3650-3310) , (3300-2485)	1684	1690	1640	3351, 3220	1128, 1031	1579	1565	1508	(1481, 773)	-	588, 575	445
(7)	(3520-3220) , (3210-3140)	3423	(3570-3280) , (3270-2445)	1644, 1635	1700, 1685	1620	3370, 3220	1129, 1031	1573	1572	1513	(1481, 773)	-	589, 570	442
(8)	(3520-3310) , (3300-3150)	3456	(3600-3320) , (3310-2780)	1632	1670	1615	3360, 3230	1128, 1033	1580	1569	1507	(1480, 772)	1444, 1335	595, 580	-
(9)	(3530-3310) , (3300-3135)	3457	(3570-3310) , (3300-2650)	1640	1675	1616	3361, 3210	1127, 1036	1582	1567	1508	(1482, 774)	1448, 1348	597, 530	-
(10)	(3530-3330) , (3320-3140)	3446	(3650-3310) , (3330-2750)	1623	1670	1610	3370, 3280	1126, 1034	1517	1568	1514	(1434, 774)	1438, 1335	598	-
(11)	(3530-3330) , (3320-3150)	3455	(3650-3310) , (3300-2750)	1623	1670	1613	3369, 3275	1126, 1036	1520	1578	1515	(1477, 775)	1451,1345	597	-
(12)	(3510-3310) , (3300-3100)	3457	(3620-3290) , (3280-2470)	1644	1671	1611	3365, 3235	1129, 1032	1587	1577	1510	(1479,774)	1441, 1333	601, 580	-
(13)	(3580-3350) , (3320-3090)	3449	(3615-3300) , (350-2450)	1648	1670	1617	3361, 3231	1129, 1035	1585	1572	1512	(1481, 777)	1442, 1347	595, 575	-
(14)	(3540-3320) , (3310-3100)	3438	(3610-3290) , (3210-2560)	1647	1673	1618	3362, 3236	1128, 1035	1586	1570	1513	(1482, 782)	1443, 1346	595, 571	-
(15)	(3530-3300) , (3290-3080)	3444	(3605-3270) , (3190-2580)	1643	1669	1611	3368, 3233	1127, 1034	1580	1571	1510	(1480, 786)	1440, 1348	595, 581	-

- **Magnetic Moments:**

The magnetic moments of the metal complexes (**2**)-(**15**) at room temperatures are shown in Table 4. Cu(II) complexes (**2**), (**3**), (**4**), (**5**), (6) and (**7**) showed values in the 1.68-1.70 B.M range corresponding to one unpaired electron in the a $d_{(x2-y2)}$ ground state in an octahedral structure. The low values than 1.73 B.M is due to spin – spin interactions tookplace between Cu(II) ions [40]. Mn(II) complexes (**14**) and (**15**) showed magnetic moment values equal to 6.18 and 6.31 B.M. These values are lower than high spin manganese (II), (d^5). This phenomenon may be due to antiferromagnetic spin- spin interactions between Mn(II) ions through molecular association or hydrogen bondings [41]. Ni(II) complexes (**12**) and (**13**) showed values equal to 3.05 and 2.98 B.M. The lowering in these values may be assigned to the interaction between the two nickel atoms via hydrogen bondings or molecular association [42]. Zn(II) complexes (**8**) and (**9**), Cd(II) complexes (**10**) and (**11**) showed diamagnetic property [43].

- **Electronic Spectra:**

The electronic spectral data for the ligand (**1**) and their metal complexes in DMSO are summarized in Table 4. The electronic absorption spectra of the ligand showed three bands located at 295, 315 and 335 nm respectively. The first one assigned to intraligand $\pi\rightarrow\pi^*$ transition in the hydroxyl moiety which is nearly unchanged on complexation. The second and third bands may be assigned to $n\rightarrow\pi^*$ and charge transfer transitions of the carboxylic and carbonyl groups. The location of these bands was found to be shifted to higher energy on complexation. This finding indicated to the participation of these groups in bonding and coordination with metal ions [44]. Copper(**II**) complexes (**2**), (**3**), (**4**), (**5**), (**6**) and (**7**) showed bands in the 296-265, 361-310, 463-435, 565-531 and 647-620 nm ranges, were assigned to intraligand transition O→Cu, charge transfer, $^2B_1\rightarrow{}^2E$ and $^2B_1\rightarrow{}^2B_2$ transitions, indicating distorted octahedral structure [45]. Manganese(**II**) complexes (**14**) and (**15**) showed bands at 282, 291, 314, 321, 337, 416, 528 and 621 and 285, 290, 312, 323, 335, 415, 55 and 623 nm, the first three bands are within the ligand and the other bands are corresponding to $^6A_{g1}\rightarrow{}^4E_g$, $^6A_{1g}\rightarrow{}^4T_{2g}$ and $^6A_{1g}\rightarrow{}^4T_{1g}$ transitions which were compatible to an octahedral geometry around the Mn(**II**) ions [46]. However, the electronic spectra of nickel(**II**) complexes (**12**) and (**13**) showed bands at 282, 295, 325, 345, 405, 460, 548, 580 and 745 nm and 283, 298, 329, 347, 410, 461, 545, 582 and 747 nm, which were assignable to intraligand transitions and $^3A_{2g}$ (F) → $^3T_{1g}$ (P) ($_3$), $^3A_{2g}$ (F) → $^3T_{1g}$ (F) ($_2$) and $^3A_{2g}$ (F) → $^3T_{1g}$ (F) ($_1$) transitions respectively, assuming the octahedral Ni(**II**) complexes [47]. The ($\upsilon_2\backslash\upsilon_1$) ratio for the complexes are less than the usual value 1.7 indicating distorted octahedral Ni(**II**) complexes, the ($\upsilon_2\backslash\upsilon_1$) value equal to 1.58 and 1.53, indicating distorted octahedral structure. Zn(**II**) complexes (**8**) and (**9**) and Cd(**II**) complexes (**10**) and (**11**) showed bands were due to intraligand transitions.

Table (4):- The electronic absorption spectral bands (nm) and magnetic moments (B.M.) for the ligand (1) and its metal complexes:

No.	λ_{max} (nm)	$_{eff}$ in B.M.	ν_2/ν_1
(1)	295nm (log ε =3.98), 315 nm (log ε =4.25) 335(log ε= 4.59)	-	-
(2)	640, 556, 438, 361, 343, 324, 295, 266	1.70	-
(3)	642, 554, 435, 360, 341, 322, 292, 265	1.69	-
(4)	647, 531, 438, 349, 336, 326, 310, 293, 279	1.70	-
(5)	640, 559, 456, 347, 329, 295, 287	1.70	-
(6)	620, 560, 461, 355, 335, 316, 296, 290	1.68	-
(7)	625, 565, 463, 360, 340, 315, 291, 285	1.69	-
(8)	321, 307, 291	Diamagnetic	-
(9)	324, 305, 290	Diamagnetic	-
(10)	326, 303, 294	Diamagnetic	-
(11)	322, 306, 292	Diamagnetic	-
(12)	745, 580, 548, 460, 405, 345, 325, 295, 282	3.05	1.58
(13)	747, 582, 545, 461, 410, 347, 329, 298, 283	2.98	1.53
(14)	621, 528, 416, 337, 321, 314, 291, 282	6.18	-
(15)	623, 525, 415, 335, 323, 312, 290, 285	6.31	-

- **Electron Spin Resonance (ESR)**

The ESR spectral data for copper(II) complexes (**3**), (**5**) and (**6**) are presented in Table **5**. The spectra of copper(II) complexes are characteristic of species d^9, configuration having axial type of a $d_{(x2-y2)}$ ground state which is the most common for copper(II) complexes. The complexes showed $g_{||}>g_{\perp}>2.0023$, indicating octahedral geometry around copper(II) ion. The g-values are related by the expression $G = (g_{||}-2)/ (g_{\perp} -2)$, where (G) exchange coupling interaction parameter (G). If G<4.0, a significant exchange coupling is present, whereas if G value > 4.0, local tetragonal axes are aligned parallel or only slightly misaligned. copper(II) Complexes showed 2.00, 2.61 and 2.7 values indicating spin-exchange interactions tookplace between copper(II) ions. This phenomenon is further confirmed by the magnetic moments values (Table (**4**)). The $g_{||}/A_{||}$ value is also considered as a diagnostic term for stereochemistry, the $g_{||}/A_{||}$ values are 155.7, 147.3 and 182.5 which are expected for distorted octahedral complexes [48]. The g-values of the copper(II) complexes with a $^2B_{1g}$ ground state ($g_{||}>g_{\perp}$) may be expressed by.

$$g_{||}=2.002 - (8K^2_{||}/\Delta E_{xy}) \quad (1)$$

$$g_{\perp}=2.002- (2K^2_{\perp}/\Delta E_{xz}) \quad (2)$$

Where $k_{||}$ and $k_{\perp}$ are the parallel and perpendicular components respectively of the orbital reduction factor (K), is the spin-orbit coupling constant for the free copper, ΔE_{xy} and ΔE_{xz} are the electron transition

energies of $^2B_{1g} \rightarrow {}^2B_{2g}$ and $^2B_{1g} \rightarrow {}^2E_g$. From the above relations, the orbital reduction factors ($K_{\|}$, $K_{\perp}$, K), which are measure terms for covalency, can be calculated. For an ionic environment, K=1; while for a covalent environment, K<1. The lower the value of K, the greater is the covalency.

$$K^2_{\perp} = (g_{\perp} - 2.002)\, \Delta E_{xz} / 2\lambda_o \quad (3)$$

$$K^2_{\|} = (g_{\|} - 2.002)\, \Delta E_{xy} / 8\lambda_o \quad (4)$$

$$K^2 = (K_{2\|} + 2K^2_{\perp})/3 \quad (5)$$

K values for the copper(II) complexes are indicating for a covalent bond character. Kivelson and Neiman noted that, for ionic environment $g_{\|} \geq 2.3$ and for a covalent environment $g_{\|} < 2.3$. Theoretical work by Smith [49] seems to confirm this view. The g-values reported here showed considerable covalent bond character. Also, the in-plane σ-covalency parameter, $\alpha^2(Cu)$ was calculated by

$$\alpha^2(Cu) = (A_{\|}/0.036) + (g_{\|} - 2.002) + 3/7(g - 2.002) + 0.04 \quad (6)$$

The calculated values suggested a covalent bonding [50]. The in-plane and out of- plane - bonding coefficients β_1^2 and β_2^2 respectively, are dependent upon the values of ΔE_{xy} and ΔE_{xz} in the following equations[58].

$$\alpha^2\beta^2 = (g_{\perp} - 2.002)\, \Delta E_{xy}/2\lambda_o \quad (7)$$

$$\alpha^2\beta_1^2 = (g_{\|} - 2.002)\, \Delta E_{xz}/8\lambda_o \quad (8)$$

In this work, the complexes show β_1^2 values indicating a moderate degree of covalency in the in-plane - bonding [51]. However, the β^2 value for complexes indicating ionic character of the out-of-plane. It is possible to calculate approximate orbital populations ford orbitals by

$$A_{\|} = A_{iso} - 2B[1 \pm (7/4)\, \Delta g_{\|}] \quad (\Delta g_{\|} = g - g_e) \quad (9)$$

$$a^2_d = 2B / 2B^{\circ} \quad (10)$$

Where A° and 2B° is the calculated dipolar coupling for unit occupancy of d orbital respectively. When the data are analyzed, the components of the Cu hyperfine coupling were considered with all the sign combinations. The only physically meaningful results are found when A and A were negative. The resulting isotropic coupling constant was negative and the parallel component of the dipolar coupling 2B are negative (Table (**5**)). These results can only occur for an orbital involving the $d_{(x2-y2)}$ atomic orbital on copper [52]. The value for 2B is quite normal for copper(II) complexes. The A_{iso} value was relatively small. The 2B value divided by $2B^{o}$ (The calculated dipolar coupling for unit occupancy of d_{x2-y2} (235.11 G), using equation (10) suggests all orbital population are 60, 66, and 57.2% d-orbital spin density respectively, clearly the orbital of the unpaired electron is $d_{(x2-y2)}$. However, Mn(II) complex (**14**) showed isotropic spectrum with g_{iso} 2.13 indicating covalent bond character [53].

Table (5):- The ESR data for metal (II) complexes:

Complex	g||	$g_{\perp}$	a_{giso}	A|| (G)	$A_{\perp}$ (G)	^{b}Aiso (G)	^{c}G	ΔE_{xy} (cm^{-1})	ΔE_{xz} (cm^{-1})	K 2 ⊥	$K_{\|}^2$	K2	K	g||/A|| (cm^{-1})	α2	β2	β2 1	- 2β	a^2d (%)
(3)	2.18	2.06	2.13	135	7.5	50	3	17241	21052	0.73	0.46	1.01	0.8	155.7	0.63	1.16	0.73	141	60
(5)	2.21	2.08	2.12	150	15	60	2.6	17544	20833	0.98	0.55	0.84	0.91	147.3	0.69	1.42	0.8	154.4	66
(6)	2.19	2.07	2.13	120	15	30	2.7	17391	21739	0.89	0.49	0.76	0.87	182.5	0.59	1.51	0.83	134	57.2
(14)	-	-	2.13	-	-	-	-	-	-	-	-	-	-	-	-	-	-	-	-

Thermal Analyses (DTA and TGA):

The thermal data of complexes (**2), (4)**, **(5), (6), (7), (8)**, **(9), (10), (12), (13) and (15)** are listed in Table 6. These complexes were introduced as representative examples. Thermogram of complex **(2)** showed decomposition in six steps, the first step involving breaking of H-bondings accompanied with endothermic peak at 46 ^{o}C. In the second step, three molecules of hydrated water molecules were lost endothermically with peak at 70 ^{o}C accompanied by 10.90% (Calc. 10.93%) weight loss. Loss of two coordinated water molecule was recorded in the third step as an endothermic peak at 155 ^{o}C with 8.10% (Calc. 8.18%) weight loss. The 29.25% weight loss (Calc. 29.21%) accompanied by an endothermic peak at 270-285 ^{o}C range was assigned to loss of coordinated 2(OAc) group, whereas the endothermic peak observed at 310 ^{o}C refered to the melting point of the complex. The final step observed as exothermic peaks at 442,495,575 and 615°C with 27.70% weight loss (Calc. 27.80%), refers to complete decomposition of the complex which exposed up with the formation of CuO. The first step observed in the thermogram of complex **(4)** involves breaking of H-bondings accompanied with endothermic peak at 48^{o}C. In the second step, two molecules of hydrated water were lost endothermically with peak at 75 accompanied by 7.30% (Calc. 7.35%) weight loss. In the third step, three molecules of coordinated water molecules were lost endothermically with a peak at 145 ^{o}C accompanied by 12.00% (Calc. 11.89%) weight loss. The forth step involved loss of coordinated (SO_4) group accompanied with an endothermic peak at 265 ^{o}C range with 24.10% (Calc. 24.00%). while the endothermic peak appeared at 315 ^{o}C refered to the melting point of the complex. The final step observed at 475,515, 590 and 605^{o}C with 26.30% weight loss (Calc. 26.15%) as exothermic peaks, refered to complete oxidative decomposition of the complex which ended up with the formation of CuO. The first step observed in the thermogram of complex **(5)** involves breaking of H-bondings accompanied with endothermic peak at 50^{o}C. In the second step, three molecules of hydrated water were lost endothermically with peak at 60 accompanied by 7.90% (Calc. 7.98%) weight loss. In the third step, one molecule of coordinated water molecules was lost endothermically with a peak at 150 ^{o}C accompanied by 2.80% (Calc. 2.89%) weight loss. The forth step involved loss of coordinated (SO_4) group accompanied with an endothermic peaks at 260, 290 ^{o}C ranges with 15.80% (Calc. 15.89%). while the endothermic peak appeared at 320 ^{o}C refered to the melting point of the complex. The final step observed at 430,465, 515 and 600^{o}C with 15.60% weight loss (Calc. 15.62%) as exothermic peaks, refered to complete oxidative decomposition of the complex which ended up with the formation of CuO. Thermogram of complex **(6)** showed decomposition in six steps, the first step involving breaking of H-bondings accompanied with endothermic peak at 45 ^{o}C. In the second step, three molecules of hydrated water molecules were lost endothermically with peak at 80 ^{o}C accompanied by 12.00% (Calc. 12.08%) weight loss. Loss of one coordinated water molecule was recorded in the third step as an endothermic peak at 160 ^{o}C with 9.10% (Calc. 9.16%) weight loss. The 19.80% weight loss (Calc. 19.89%) accompanied by an endothermic peak at 270-285 ^{o}C range was assigned to loss of coordinated 2(Cl) group, whereas the endothermic peak observed at 322 ^{o}C refered to the melting point of the complex. The final step observed as exothermic peaks at 435,480,510 and 595°C with 27.75% weight loss (Calc. 27.80%), refered to complete decomposition of the complex which exposed up with the formation of CuO. The first step observed in the thermogram of complex **(7)** involving breaking of H-bondings accompanied with endothermic peak at 47 ^{o}C. In the second step, three molecules of hydrated water were lost endothermically with peak at 72 ^{o}C accompanied by 8.60% (Calc. 8.52%) weight loss. The 12.20% weight loss (Calc. 12.24%) accompanied by an endothermic peaks appear at 273-282^{o}C was assigned to loss of coordinated 2(Cl) groups whereas the endothermic peak observed at 325 ^{o}C refered to the melting point of the complex. The final step observed at 470,535,600 and 610 ^{o}C with 15.50% weight loss (Calc. 15.62%), refers to complete oxidative decomposition of the complex which exposed up with the formation of CuO. Thermogram of complex **(8)** showed decomposition in six steps, the first step involving breaking of H-bondings accompanied with endothermic peak at 46 ^{o}C. In the second step, three molecules of hydrated water molecules were lost endothermically with peak at 73 ^{o}C accompanied by 10.80% (Calc. 10.89%) weight loss. Loss of two coordinated water molecule was recorded in the third step as an endothermic peak at 155 ^{o}C with 8.10% (Calc. 8.14%) weight loss. The 29.10% weight loss (Calc. 29.06%) accompanied by an endothermic peak at 260-275 ^{o}C range was assigned to loss of

coordinated 2(OAc) group, whereas the endothermic peak observed at 333 ^{o}C refered to the melting point of the complex. The final step observed as exothermic peaks at 420,480,530 and 615°C with 28.20% weight loss (Calc. 28.13%), refered to complete decomposition of the complex which exposed up with the formation of ZnO. Thermogram of complex **(9)** showed decomposition in five steps, the first step involving breaking of H-bondings accompanied with endothermic peak at 49 ^{o}C. In the second step, three molecules of hydrated water molecules were lost endothermically with peak at 80 ^{o}C accompanied by 7.90% (Calc 7.91%) weight loss. The 18.70% weight loss (Calc. 18.76%) accompanied by an endothermic peak at 275-280 ^{o}C range was assigned to loss of coordinated 2(OAc) group, whereas the endothermic peak observed at 335 ^{o}C refered to the melting point of the complex. The final step observed as exothermic peaks at 445,490,545 and 600°C with 15.80% weight loss (Calc. 15.85%), refered to complete decomposition of the complex which exposed up with the formation of ZnO. Thermogram of complex **(10)** showed decomposition in six steps, the first step involving breaking of H-bondings accompanied with endothermic peak at 45 ^{o}C. In the second step, three molecules of hydrated water molecules were lost endothermically with peak at 60 ^{o}C accompanied by 9.90% (Calc. 9.94%) weight loss. Loss of two coordinated water molecule was recorded in the third step as an endothermic peak at 145 ^{o}C with 7.30% (Calc. 7.36%) weight loss. The 26.10% weight loss (Calc. 26.05%) accompanied by an endothermic peak at 280-295 ^{o}C range was assigned to loss of coordinated 2(OAc) group, whereas the endothermic peak observed at 314 ^{o}C refered to the melting point of the complex. The final step observed as exothermic peaks at 445,495,520 and 585°C with 38.30% weight loss (Calc. 38.21%), refered to complete decomposition of the complex which exposed up with the formation of CdO. Thermogram of complex **(12)** showed decomposition in six steps, the first step involving breaking of H-bondings accompanied with endothermic peak at 49 ^{o}C. In the second step, three molecules of hydrated water molecules were lost endothermically with peak at 70 ^{o}C accompanied by 11.10% (Calc. 11.04%) weight loss. Loss of two coordinated water molecule was recorded in the third step as an endothermic peak at 165 ^{o}C with 8.40% (Calc. 8.28%) weight loss. The 29.50% weight loss (Calc 29.57%) accompanied by an endothermic peak at 270-285 ^{o}C range was assigned to loss of coordinated 2(OAc) groups, whereas the endothermic peak observed at 338 ^{o}C refered to the melting point of the complex. The final step observed as exothermic peaks at 460,530,575 and 615°C with 26.30% weight loss (Calc 26.33%), refered to complete decomposition of the complex which exposed up with the formation of NiO. The first step observed in the thermogram of complex **(13)** involving breaking of H-bondings accompanied with endothermic peak at 46 ^{o}C. In the second step, three molecules of hydrated water were lost endothermically with peak at 80^{o}C. Accompanied by % 8.00 (Calc. 8.04%) weight loss. The 18.90% weight loss (Calc. 18.97%) accompanied by an endothermic peak at 260-280 ^{o}C range was assigned to loss of coordinated 2(OAc) groups, whereas the endothermic peak observed at 340 ^{o}C refered to the melting point of the complex. The final step observed at 445,490,540 and 610°C with 14.60% weight loss (Calc. 14.68%), refered to complete oxidative decomposition of the complex which exposed up with the formation of NiO. The first step observed in the thermogram of complex **(15)** involving breaking of H-bondings accompanied with endothermic peak at 50 ^{o}C. In the second step, three molecules of hydrated water were lost endothermically with peak at 80^{o}C accompanied by % 8.10 (Calc. 8.04%) weight loss. The 19.10% weight loss (Calc. 19.09%) accompanied by an endothermic peak at 255-275 ^{o}C range was assigned to loss of coordinated 2(OAc) groups, whereas the endothermic peak observed at 330 ^{o}C refered to the melting point of the complex. The final step observed at 455,495,555 and 620°C with 14.10% weight loss (Calc. 14.20%), refered to complete oxidative decomposition of the complex which exposed up with the formation of MnO [54-56].

Table (6): Thermal analyses for some metal (II) complexes:

Compound No. Molecular formula	Temp. (°C)	DTA (peak)		TGA (Wt.loss %)		Assignments
		Endo	Exo	Calc	Found	
Complex (2)	46	endo	-	-	-	Broken of H-bondings
	70	endo	-	10.93	10.90	Loss of ($3H_2O$) hydrated water molecules
	155	endo	-	8.18	8.10	Loss of ($2H_2O$) coordinated water molecule
	270,285	endo	-	29.21	29.25	Loss of coordinated 2(OAc) group
	310	endo	-	-	-	Melting point
	442,495,575,615	-	Exo	27.80	27.70	Decomposition process with the formation of (CuO)
Complex (4)	48	endo	-	-	-	Broken of H-bondings
	75	endo	-	7.35	7.30	Loss of ($2H_2O$) hydrated water molecule
	145	endo	-	11.89	12.00	Loss of ($3H_2O$) coordinated water molecule
	265	endo	-	24.00	24.10	Loss of coordinated (SO_4)group
	315	endo	-	-	-	Melting point
	475,515,590,605	-	Exo	26.15	26.30	Decomposition process with the formation of (CuO)
Complex (5)	50	endo	-	-	-	Broken of H-bondings
	60	endo	-	7.98	7.90	Loss of ($3H_2O$) hydrated water molecule
	150	endo	-	2.89	2.80	Loss of (H_2O) coordinated water molecule
	260,290	endo		15.87	15.80	Loss of coordinated SO_4 group
	320	endo	-	-	-	Melting point
	430,465,515,600	-	Exo	15.62	15.60	Decomposition process with the formation of (CuO)
Complex (6)	45	endo	-	-	-	Broken of H-bondings
	80	endo	-	12.08	12.00	Loss of ($3H_2O$) hydrated water molecule
	160	endo	-	9.16	9.10	Loss of (H_2O) coordinated water molecule
	270,285	endo		19.89	19.80	Loss of coordinated 2 (Cl) group
	322	endo	-	-	-	Melting point
	435,480,510,595	-	Exo	27.80	27.75	Decomposition process with the formation of (CuO)
Complex (7)	47	endo	-	-	-	Broken of H-bondings
	72	endo	-	8.52	8.60	Loss of ($3H_2O$) hydrated water molecule
	273,282	endo	-	12.24	12.20	Loss of coordinated 2 (Cl) group
	325	endo	-	-	-	Melting point
	470,535,600,610	-	Exo	15.62	15.50	Decomposition process with the formation of (CuO)
Complex (8)	46	endo	-	-	-	Broken of H-bondings
	73	endo	-	10.89	10.80	Loss of ($3H_2O$) hydrated water molecule
	155	endo	-	8.14	8.10	Loss of ($2H_2O$) coordinated water molecule
	260,275	endo	-	29.06	29.10	Loss of coordinated 2(OAc) group
	333	endo	-	-	-	Melting point
	420,480,530,615	-	Exo	28.13	28.20	Decomposition process with the formation of (ZnO)
Complex (9)	49	endo	-	-	-	Broken of H-bondings
	80	endo	-	7.91	7.90	Loss of ($3H_2O$) hydrated water molecule
	275,280	endo	-	18.76	18.70	Loss of coordinated 2 (OAc) group
	335	endo	-	-	-	Melting point
	445,490,545,600	-	Exo	15.85	15.80	Decomposition process with the formation of (ZnO)
Complex (10)	45	endo	-	-	-	Broken of H-bondings
	60	endo	-	9.94	9.90	Loss of 3(H_2O) hydrated water molecules
	145	endo	-	7.36	7.30	Loss of 2(H_2O) coordinated water molecules
	280,295	endo	-	26.05	26.10	Loss of coordinated 2(OAc) group
	314	endo	-	-	-	Melting point
	445,495,520,585	-	Exo	38.21	38.30	Decomposition process with the formation of (CdO)

Compound No. Molecular formula	Temp. (^{o}C)	DTA (peak)		TGA (Wt.loss %)		Assignments
		Endo	Exo	Calc	Found	
Complex (12)	49	endo	-	-	-	Broken of H-bondings
	70	endo	-	11.04	11.10	Loss of ($3H_2O$) hydrated water molecule
	165	endo	-	8.28	8.40	Loss of ($2H_2O$) coordinated water molecule
	270,285	endo	-	29.57	29.50	Loss of coordinated 2(OAc) group
	338	endo	-	-	-	Melting point
	460,530,575,615	-	Exo	26.33	26.30	Decomposition process with the formation of (NiO)
Complex (13)	46	endo	-	-	-	Broken of H-bondings
	80	endo	-	8.04	8.00	Loss of ($3H_2O$) hydrated water molecule
	260,280	endo		18.97	18.90	Loss of coordinated 2(OAc) group
	340	endo	-	-	-	Melting point
	445,490,540,610	-	Exo	14.68	14.60	Decomposition process with the formation of (NiO)
Complex (15)	50	endo	-	-	-	Broken of H-bondings
	80	endo	-	8.04	8.10	Loss of ($3H_2O$) hydrated water molecule
	255,275	endo	-	19.09	19.10	Loss of coordinated 2 (OAc) group
	330	endo	-	-	-	Melting point
	455,495,555,620	-	Exo	14.20	14.10	Decomposition process with the formation of (MnO)

^{1}H-NMR spectra:

^{1}H-NMR spectra of the ligand (**1**) and some of its metal complexes, such as Zn**(II)** complexes (**8**), (**9**) and Cd**(II)** complexes (**10**), (**11**). The spectrum of the ligand showed peak at 11.220 p.p.m is due to proton of aromatic OH group. However, the protons of aromatic ring appeared as multiplets peaks in the 6.902 - 8.057 p.p.m range and another one at 9.201 p.p.m corresponds to proton of NH_2 group. When deuterated DMSO is used as a solvent, the OH protons were disappeared, since D(^{2}H) does not show up in the ^{1}H-NMR spectrum. The protons of methyl group attached to carbonyl group appeared at 3.158 p.p.m. The spectrum of Zn**(II)** complex (**8**) showed OH proton at 11.111 p.p.m. The protons of aromatic rings appeared in the 6.694 - 8.105 p.p.m range and another one at 8.991 p.p.m corresponds to proton of NH_2 group. However, the methyl protons attached to carbonyl and acetate groups observed at 3.481 and 1.847 p.p.m respectively. The spectrum of Zn**(II)** complex (**9**) showed OH proton at 10.695 p.p.m. The protons of aromatic rings appeared in the 6.799 - 8.103 p.p.m range and another one at 8.775 p.p.m corresponds to proton of NH_2 group . However, the methyl protons attached to carbonyl and acetate groups observed at 3.155 and 2.501 p.p.m respectively.The spectrum of Cd**(II)** complex (**10**) shows OH proton at 10.555 p.p.m. The protons of aromatic rings appeared in the 6.727 – 7.569 p.p.m range and another one at 8.565 p.p.m corresponds to proton of NH_2 group. However the methyl protons attached to carbonyl and acetate groups observed at 3.381 and 2.494 p.p.m respectively. The spectrum of Cd**(II)** complex (**11**) shows OH proton at 10.765 p.p.m. The protons of aromatic rings appeared in the 6.753 – 7.594 p.p.m range and another one at 8.899 p.p.m corresponds to proton of NH_2 group. However the methyl protons attached to carbonyl and acetate groups observed at 3.391 and 2.499 p.p.m respectively [57].

Antimicrobial activity:

In vitro biological screening test of the ligand (**1**) and its metal complexes **(2), (3), (4), (6), (8), (10), (11), (12)** and **(14)** carried out as antibacterial and antifungal activity (Figures **3** and **4**). The antibacterial activity was tested against two bacterial strains; Gram-positive *Staphylococcus aureus* as well as Gram-negative *Escherichia coli* strains [58-60]. The results compared with standard drug Ampicllin (Gram positive) and Amphotericin **B** (Gram negative). The complexes were also subjected to antifungal activity against *Aspergillus flavus* and *Candida albicans* with standard drug. The data indicated that, using low concentration against microbes, aspirin and ligand no effect was observed, however, the complexes show moderate to high effect, The order for Gram positive is Cd(**II**) complex (**10**)> Cd(**II**) complex (**11**)>

ampicillin> Zn(**II**) complex (**8**)> Cu(**II**) complex (**4**)> Cu(**II**) complex (**6**)= Ni(**II**) complex (**12**)> Cu(**II**) complex (**2**) = Cu(**II**) complex (**3**)> ligand**(1)**> aspirin> Mn(**II**)complex(**14**) and for Gram negative is ampicillin> Cd(**II**) complex (**10**)> Cd(**II**) complex (**11**)> Cu(**II**) complex (**2**) > Cu(**II**) complex (**6**)> Cu(**II**) complex (**3**)> Cu(**II**) complex (**4**) > Zn(**II**) complex (**8**)> aspirin> Ni(**II**) complex (**12**) > ligand (**1**)> Mn(**II**) complex (**14)** and for *Aspergillus flavus* is Cd(**II**) complex (**10**)>amphotericin B> Cd(**II**) complex (**11**)> ligand (**1**)= aspirin= Cu(**II**) complex (**2**)= Cu(**II**) complex (**3**)= Cu(**II**) complex (**4**)= Cu(**II**) complex (**6**) = Zn(**II**) complex (**8**)= Ni(**II**) complex (**12**)= Mn(**II**) complex (**14**) and for *Candida albicans* is Cd(**II**) complex (**10**) > Cd(**II**) complex (**11**)> amphotericin B > Ni(**II**) complex (**12**)> Cu(**II**) complex (**3**)= Cu(**II**) complex (**6**)> Cu(**II**) complex (**2**)= Cu(**II**) complex (**4**)> ligand**(1)** = aspirin= Zn(**II**) complex (**8**)= Mn(**II**) complex (**14**). Invivo studies showed no toxicity was observed for all organs tested. The major groups of antibiotics that are currently in use have three microbial targets: the cell wall synthesis, translational machinery and DNA replication machinery. Unfortunately, microbial resistance can develop against each of these modes of action. Most of the antibiotic resistance mechanisms are irrelevant for nanoparticles (NPs) because the mode of action of NPs is direct contact with the microbial cell wall without the need to penetrate the cell. This raises the hope that NPs would be less prone to promote resistance in microbes than antibiotics. Most microbes exist in the form of a biofilm which often contains diverse species that interact with each other and their environment. Biofilms are specifically microbial aggregates that rely on a solid surface and extracellular products, such as extracellular polymeric substances (EPSs).Microbes move reversibly onto the surface but the expression of EPSs renders the attachment irreversible. Once the microbes settled, synthesis of the microbial flagellum is inhibited and the microbes multiply rapidly resulting in the development of a mature biofilm. At this stage, the microbes are stuck together, forming a barrier that can resist antibiotics and provide a source of systemic chronic infections, thus, biofilm are a serious health threat. Nano materials are materials that have at least one dimension (**1-100**nm) in the nanometer scale. NPs have demonstrated broad-spectrum antimicrobial properties. The antimicrobial mechanism of action of NPs is generally described as adhering to one of three models: oxidative stress induction, metal ion release, or non-oxidative mechanism. These three types of mechanisms can occur simultaneously. Nano Cd**(II)** complex (**10**) showed higher activity compared with the standard and other complexes. It may be Cd**(II)** complex prompt neutralization of the surface electric charge of the microbial membrane and change its penetrability, ultimately leading to microbial death [61, 62]. In vitro antibacterial and antifungal activity of the ligand (**1**), Aspirin and some metal complexes were shown in Table (**7**).

Table (7): In vitro antibacterial and antifungal activity of ligand (1), aspirin and some metal complexes

	Escherichia coli(G-)	*Staphylococcus aureus(G+)*	*Aspergillus flavus*	*Candida*
Control: DMSO	0	0	0	0
Ampicillin Antibacterial agent	25	21	0	0
Amphotericin B	0	0	17	21
Aspirin	13	11	0	0
ligand (**1**)	10	12	0.0	0.0
Cu(**II**) complex (**2**)	15	14	0.0	9
Cu (**II**) complex (**3**)	14	14	0.0	10
Cu (**II**) complex (**4**)	14	16	0.0	9
Cu (**II**) complex (**6**)	15	15	0.0	10
Zn (**II**) complex (**8**)	14	19	0.0	0.0
Cd (**II**) complex (**10**)	24	24	20	26
Cd (**II**) complex (**11**)	17	22	17	22
Ni (**II**) complex (**12**)	12	15	0.0	17
Mn (**II**) complex (**14**)	9	10	0.0	0.0

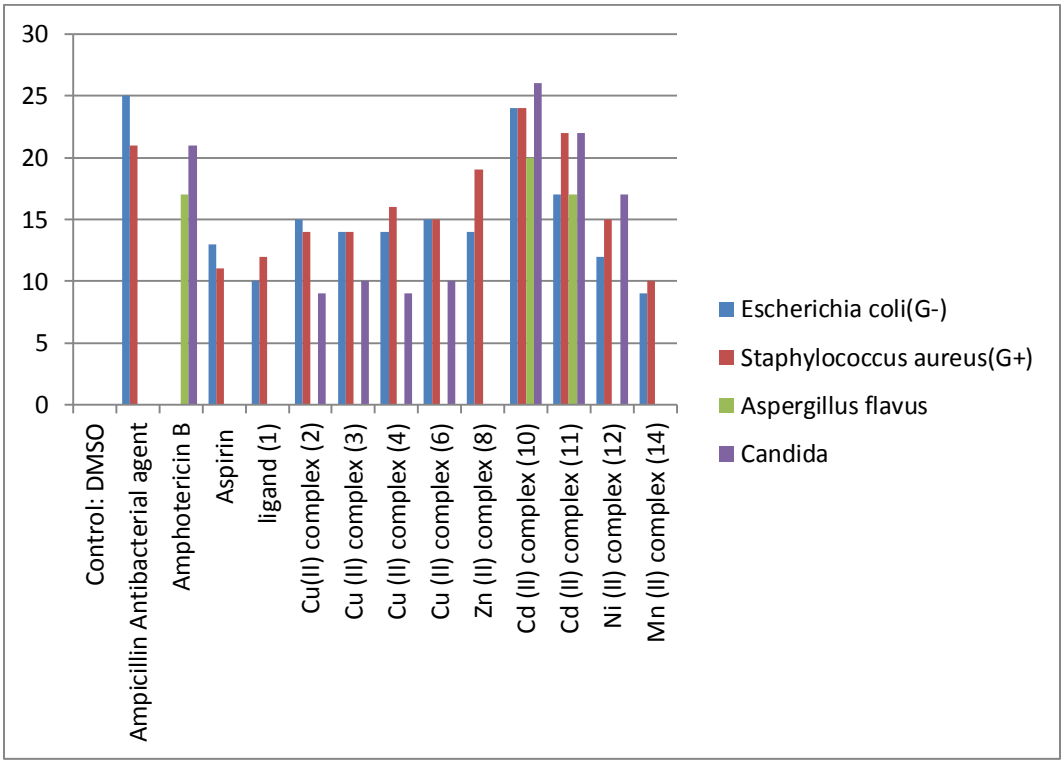

Figure (**3**): In vitro antibacterial and antifungal activity of ligand (**1**), Aspirin and some metal complexes

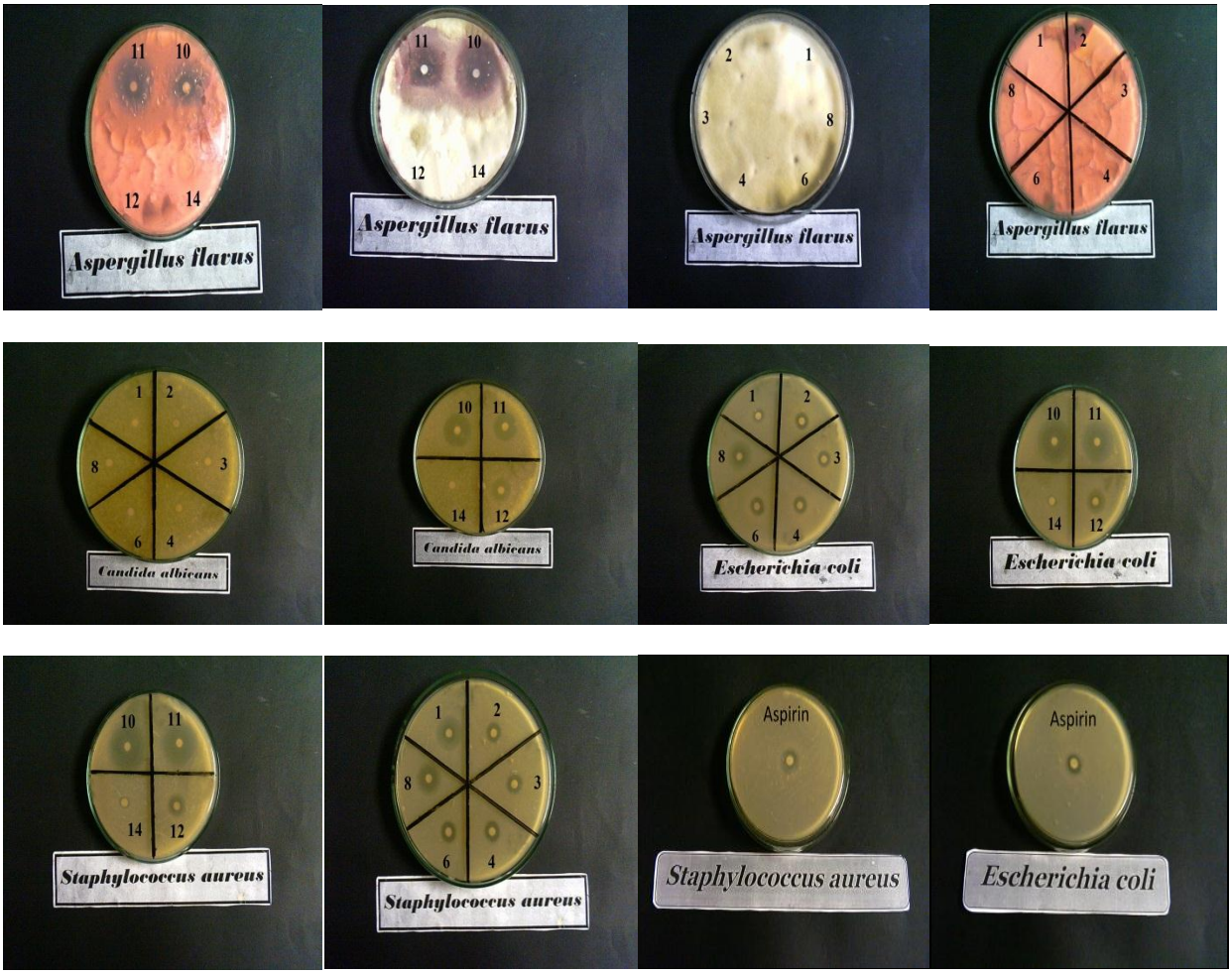

Figure (**4**): In vitro antibacterial and antifungal diagram of the ligand (**1**), aspirin and some metal complexes.

In vivo toxicity studies

Determination of liver functions AST, ALT, and albumin in the serum of normal rats showed no significant differences between treated groups and the control group. Also, there are no any significant differences in renal functions or hematological parameters between all tested groups.

Catalytic effect:

The decomposition of H_2O_2 was used as a model for the oxidation-reduction reaction to measure the catalytic effect of the prepared complexes (**2**), (**4**), (**6**), (**12**) and (**14**). The decomposition reaction was found to follow a first-order reaction kinetics. The decomposition data of H_2O_2 over the tested complexes are shown in figure (**5**). The data are plotted as ln a/ (a-x) versus time, where **"**a**"** is the initial concentration of H_2O_2 and **"**x**"** is the concentration after time t. the rate constant values for the complexes are 0.014 Cu(**II**) complex (**2**), 0.02 Cu(**II**) complex (**6**), 0.033 Cu(**II**) complex (**4**), .036 Ni(**II**) complex (**12**) and 0.043 Mn(**II**) complex (**14**) respectively. As shown in figure (**5**), although the all complexes are octahedral geometry, the catalytic effect belongs to the nature of the metal ion and anions. Previous researches reported that M^{+2}/M^{+} system formed catalytic active site. The M^{+} was identified as the species

which control the catalytic activity of the complexes [63]. The order of the catalytic effect is Mn(**II**) complex (**14**) > Ni(**II**) complex (**12**) > Cu(**II**) complex (**4**) > Cu(**II**) complex (**6**)> Cu(**II**) complex (**2**) respectively. The decomposition of H_2O_2 in the presence of the complex may be represented as follows:-

$H_2O_2 \rightarrow H^+ + HO^-_2$ **(1)**

$HO^-_2 \rightarrow HO_2 + e$ **(2)**

$M^{2+} + e \rightarrow M^+$ **(3)**

$M^+ \rightarrow M^{2+} + e$ **(4)**

$H^+ + e \rightarrow H$ **(5)**

$H_2O_2 \rightarrow H_2O + ½ O_2$ **(6)**

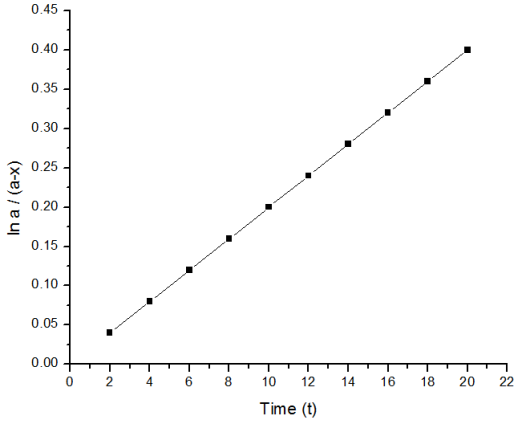

Cu(**II**) complex (**2**)

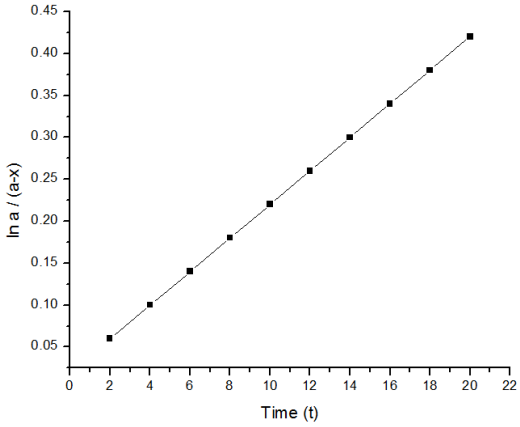

Cu(**II**) complex (**6**)

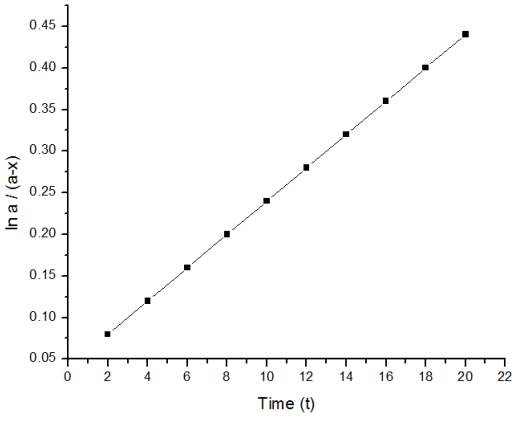

Cu(**II**) complex (**4**)

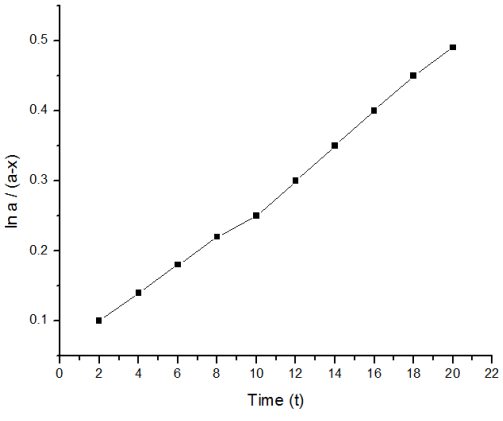

Ni(**II**) complex (**12**)

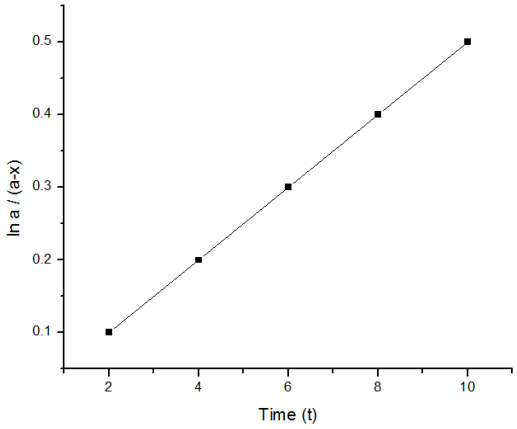

Mn(**II**) complex (**14**)

Figure (**5**):- Decomposition of H_2O_2 on tested complexes at room temperature.

Conclusion

In this paper, we are trying to focus attention on the synthesis of new compounds. These new compounds have a considerable importance in medicinal chemistry due to their broad spectrum as anti-inflammatory, anti-bacterial and anti-fungal agents. We also give spots on the target compound, complex (**10**) because of its nano structure which gives it a great possibility to be used as anti-viral drug.

References:-

1) H. Ilkimen, C. Yenikaya, M. Sart, M. Bulbul, E. Tunca and H. Dal, (2014). Synthesis and characterization of a proton transfer salt between 2,6-pyridinedicarboxylic acid and 2-aminobenzothiazole, and its complexes and their inhibition studies on carbonic anhydrase isoenzymes, Journal of enzyme inhibition and medicinal chemistry 29 (3), 353-361.
2) M. N. Deodhar, A. C. Dongre and S. D. Kudale, (2012). Analgesic and Antiinflammatory Activity of Derivatives of 2-Aminobenzothiazole Asian Journal of Chemistry, 24 (6), 2747- 2752.
3) A. Sukul, S. K. Poddar, S. Haque, S. K. Saha, S. C. Das, Z. Al Mahmud and S. M. Adur Rahman, (2017). Synthesis, Characterization and Comparison of Local Analgesic, Anti-Inflammatory, Anti-Ulcerogenic Activity of Copper and Zinc Complexes of Indomethacin. Anti-inflammatory & Anti-allergy Agents in Medicinal Chemistry, 15 (3), 221- 233.

4) I. Lakovidis, I. Delimaris and S. M. Piperakis, (2011). Copper and Its Complexes in Medicine: A Biochemical Approach, Molecular Biology International, vol (2011), 13.
5) Thompson, K. H., Orvig, C. (2003). Boon and Bane of Metal Ions in Medicine. Science, vol 300 (5621), 936- 939.
6) Regiel-Futyra, A., Da˛browski, J.M., Mazuryk, O., Spiewak, K., Kyzioł, A., Pucelik, B., Brindell, M., Stochel, G. (2017). Bioinorganic antimicrobial strategies in the resistance era, Coordination. Chemistry. Reviews, 351, 76-117.
7) Guerra, W., Silva-Caldeira, P.P., Terenzi, H., Pereira-Maia, E.C. (2016). Impact of metal coordination on the antibiotic and non-antibiotic activities of tetracyclinebased drugs, Coordination. Chemistry. Reviews, 327-328, 188-199.
8) Mohler, J.S., Kolmar, T., Synnatschke, K., Hergert, M., Wilson, L.A., Ramu, S., Elliott, A.G., Blaskovich, M.A.T., Sidjabat, H.E., Paterson, D.L. (2017). Enhancement of antibiotic-activity through complexation with metal ions-combined ITC, NMR, enzymatic and biological studies, Journal of Inorganic and Biochemistry, 167, 134-141.
9) Yu, M., Nagalingam, G., Ellis, S., Martinez, E., Sintchenko, V., Spain, M., Rutledge, P.J., Todd, M.H., Triccas, J.A. (2016). Nontoxic metal-cyclam complexes, a new class of compounds with potency against drug-resistant Mycobacterium tuberculosis, Journal of Medicinal Chemistry, (59), (12), 5917-5921.
10) Shahabadi, N., Shiri, F., Hadidi, S. (2019). Studies on the interaction of antibiotic drug Rifampin with DNA and influence of bivalent metal ions on binding affinity, Spectrochim. Acta A Mol. Biomol. Spectrosc, (219), 195-201.
11) Nazir, S., Anwar, J., Munawar, M.A., Qazi, J.I., Best, S.P., Cheah, M. Yaseen, M. (2018). Metal complexation induces antibiotic activity in SEthyl-l-Cysteine sulfoxide, Inorg. Chim. Acta, (478), 166-175.
12) Williamson, K.L., Macroscale, M. (1994). Organic Experiments, Houghton Mifflin, Boston, Mass, USA, 2nd edition.
13) Ngaini, Z., Mohd A.M.A., Hussain, H., Mei, E.S., Tang, D., Kamaluddin, D.H.A. (2012). "Synthesis and antibacterial activity of acetoxybenzoyl thioureas with aryl and amino acid side chains," Phosphorus, Sulfur and Silicon and the Related Elements, (187), (1), 1–7.
14) Lawal, A., Obaleye, J. A. (2007). "Synthesis, characterization and antibacterial activity of aspirin and paracetamol-metal complexes," Biokemistri, (19), (1), 9–15.
15) Chavan, A.B., Chitte, P. D., Choudhary, N. P., Albhar, K. G., Hukkeri, V. I. (2012). "Synthesis and biological evaluation of novel benzimidazole derivative with aspirin as potent antimicrobial & antifungal agents," International Journal of Scientific Research and Reviews, (1), 22–30.
16) Bratasz, K., Selvendiran, T., Wasowicz. (2008). "NCX-4040, a nitric oxide-releasing aspirin, sensitizes drug-resistant human ovarian xenograft tumors to cisplatin by depletion of cellular thiols," Journal of Translational Medicine, (6), (9).
17) Joseph, S., Nie, T., Huang, L. (2011). "Structure-activity relationship study of novel anticancer aspirin-based compounds," Molecular Medicine Reports, (4), (5), 891–899.
18) Friedman, A.J., Grote, E.C., Meckfessel, M.H. (2016). Urea: a clinically oriented overview from bench to bedside. J Drugs Dermatol, (15), 633-639.
19) Voegeli, D. (2012). Urea creams in skin conditions: composition and outcomes. Dermatol Pract, (18), 13-15.

20) Wohlrab, W. (1984). The influence of urea on the penetration kinetics of topically applied corticosteroids. Acta Derm Venereol, (64), 233-238.
21) Marion, L.G., Krum, R. (1979). Specialized vehicles to augment percutaneous penetration of topical steroids. Curr Ther Res, (25), 56-66.
22) Dars, S., Banwell, H.A., Matricciani, L. (2019). The use of urea for the treatment of onychomycosis: a systematic review. J Foot Ankle Res, 12-22.
23) Vogel, A. (1978). A Text Book of Quantitative Inorganic Analysis, London: ELBS.
24) Figgis, B., Lewis, J., Wilkins, R. (1960). Modern Coordination Chemistry, New York: Interscience.
25) Vichai, V., Kirtikara, K. (2006). Sulforhodamine B colorimetric assay for cytotoxicity screening, Nature Protocols, 1: 1112-1116.
26) Nagesh, G., Mruthyunjayaswamy, B. (2015). Synthesis, characterization and biological relevance of some metal (II) complexes with oxygen, nitrogen and oxygen (ONO) donor Schiff base ligand derived from thiazole and 2-hydroxy- 1-naphthaldehyde, Journal of Molecular Structure, 1085: 198-206.
27) El-Tabl A. S., Abd-El Wahed M. M., Ahmed, R.A.S., Sarhan, K.S. (2020). Synthesis and structural characterization of new and exciting NP complexes-based paracetamol moiety with antimicrobial activity Journal of Chemistry and Chemical Sciences, 10(1), 32-64.
28) El-Tabl, A. S., Abd-El Wahed, M.M., Ashour, A.M., Ahmed, R.A.S. (2021). The new acetaminophen drug in the form of nano-organometallic compounds as a bright future for antimicrobial therapy, Drug designing open access, 10(2), 174.
29) Grün, B., Zeileis, A. (2009). Automatic Generation of Exams in R. Journal of Statistical Software, 29(10), 1–14.
30) Geary, W. J. (1971). The use of conductivity measurements in organic solvents for the characterisation of coordination compounds, Coordination Chemistry Reviews,7, 81-122.
31) Pouralimardan, O., Chamayou, A. C., Janiak, C., Hosseini, M. H. (2007). Hydrazone Schiff-base-manganese(II) complexes: Synthesis, crystal structure and catalytic reactivity, Inorganica Chimica Acta, 360, 1599-1608.
32) Babu, S. V., Reddy, K. H. (2013). Second derivative spectrophotometric determination of copper (II) using 2-acetylpyridine semicarbazone in biological, leafy vegetable and synthetic alloy samples, Indian Journal of Advances in Chemical Science, 1, 105-111.
33) Chanu, O. B., Kumar, A., Ahmed, A., Lal, R. (2012). Synthesis and characterisation of heterometallic trinuclear copper(II) and zinc(II) complexes derived from bis (2-hydroxy-1-naphthaldehyde) oxaloyldihydrazone, Journal of Molecular Structure, 1007, 257-274.
34) Fouda, M. F., Abd-Elzaher, M. M., Shakdofa, M. M., El-Saied, F. A., Ayad, M. I., El Tabl, A. S. (2008). Synthesis and characterization of a hydrazone ligand containing antipyrine and its transition metal complexes, Journal of Coordination Chemistry, 61, 1983-1996.
35) Gudasi, K.B., Patil, M.S.,Vadavi, R.S., Shenoy, R.V., Patil, S.A., Nethaji, M. (2006). X-ray crystal structure of the N-(2-hydroxy- 1-naphthalidene) phenylglycine Schiff base. Synthesis and characterization of its transition metal complexes, Transition Metal Chemistry, 31, 580-585.
36) Hong, M., Yin, H., Zhang, X., Li, C., Yue, C., Cheng, S. (2013). Di-and tri-organotin (IV) complexes with 2-hydroxy-1-naphthaldehyde 5-chloro-2-hydroxybenzoylhydrazone: Synthesis, characterization and in vitro antitumor activities, Journal of Organometallic Chemistry, 724, 23-31.

37) El-Wahab, Z.A., Mashaly, M.M., Salman, A., El-Shetary, B., Faheim, A. (2004). Co(II), Ce(III) and uo2 (VI) bis-salicylatothiosemicarbazide complexes: Binary and ternary complexes, thermal studies and antimicrobial activity, Spectrochimica Acta Part A: Molecular and Biomolecular Spectroscopy, 60, 2861-2873.
38) El-Tabl, A.S., Shakdofa, M.M. (2013). Metal complexes of N'-(2-hydroxy-5-phenyldiazenyl) benzylideneisonicotinohydrazide: Synthesis, spectroscopic characterization and antimicrobial activity, Journal of the Serbian Chemical Society, 78, 39-55.
39) Saied, E., Fathy, A., Shakdofa, M.M., El-Tabl, A.S., Abd Elzaher, M.M. (2014). Coordination behaviour of N′ 1, N′ 4‐bis ((1, 5‐dimethyl‐3‐ oxo-2-phenyl-2, 3-dihydro-1H-pyrazol-4-yl) methylene) succinohydrazide toward transition metal ions and their antimicrobial activities, Main Group Chemistry, 13(2), 87-103.
40) El-Tabl, A.S. (2002). Synthesis, characterisation and antimicrobial activity of manganese(II), nickel(II), cobalt(II), copper(II) and zinc(II) complexes of a binucleating tetradentate ligand, Journal of Chemical Research, 529-531.
41) Xiang, G.Q., Zhang, L.X., Zhang, A.J., Cai, X.Q., Hu, M.L. (2004). 6‐(2, 4‐Difluorophenyl)‐3‐(3‐ methylphenyl)-7H-1, 2, 4-triazolo [3, 4-b][1, 3, 4] thiadiazine, Acta Crystallographica Section E: Structure Reports Online, 60, 2249-2251.
42) Goel, S., Chandra, S., Dwivedi, S.D. (2013). Synthesis, spectral and biological studies of copper(II) and iron(III) complexes derived from 2-acetyl benzofuran semicarbazone and 2-acetyl benzofuran thiosemicarbazone, Journal of Saudi Chemical Society, 1319-6103.
43) El-wakiel, N., El-keiy, M., Gaber, M. (2015). Synthesis, spectral, antitumor, antioxidant and antimicrobial studies on Cu(II), Ni(II) and Co (II) complexes of 4-[(1H-Benzoimidazol-2-ylimino)- methyl]-benzene-1, 3-diol, Spectrochimica Acta Part A: Molecular and Biomolecular Spectroscopy, 147, 117-123.
44) El-Tabl, A.S., El-Enein, S.A. (2004). Reactivity of the new potentially binucleating ligand,2-(acetichydrazido-N-methylidene-α-naphthol)- benzothiazol, towards manganese(II), nickel(II), cobalt(II), copper(II) and zinc(II) salts, Journal of Coordination Chemistry, 57, 281-294.
45) El-Tabl, A.S., Shakdofa, M.M.E., Whaba, M.A. (2015). Synthesis, characterization and fungicidal activity of binary and ternary metal(II) complexes derived from 4,4′‐((4‐nitro‐1,2‐phenylene) bis(azanylylidene))bis(3-(hydroxyimino)pentan-2-one) Spectrochimica Acta Part A: Molecular and Biomolecular Spectroscopy, 136, 1941-1949.
46) El-Tabl, A.S., El-Saied, F.A., Ayad, M.I. (2002). Manganese(II), iron(III), cobalt(II), nickel(II), copper(II), zinc(II), and uranyl(VI) complexes of n-(2-furylidene) benzothiazol- 2-ylacet ohydrazide, Synthesis and Reactivity in Inorganic and Metal-Organic Chemistry, 32, 1189-1203.
47) El-Tabl, A.S. (2004). Synthesis and characterization of cobalt(II)/(III), nickel(II) and copper(II) complexes of new 14, 15 and 16-membered macrocyclic ligands, Bulletin of the Korean Chemical Society, 25, 1757-1763.
48) El-Boraey, H., El-Tabl, A. (2003). Supramolecular copper(II) complexes with tetradentate ketoenamine ligands, Polish Journal of Chemistry, 77, 1759-1775.
49) Ray, R., Kauffmann, G.B. (1990). An EPR study of copper (II)-substituted biguanide complexes. Part III, Inorganica Chimica Acta, 174, 237-244.
50) El-Tabl, A.S. (2004). Synthetic and spectroscopic investigations of some transition metal complexes of hydroxy-oxime ligand, Journal of Chemical Research, 19-22.

51) El-Tabl, A.S. (1997). An esr study of copper(II) complexes of N-hydroxyalkylsalicylideneimines, Transition Metal Chemistry, 23, 63-65.
52) Al-Hakimi, A.N., Shakdofa, M.M., El-Seidy, A.M., El-Tabl, A.S. (2011). N, N 2-bis (3-((3-hydroxynaphthalen-2-yl) methylene- amino) propyl) phthalamide, Journal of the Korean Chemical Society, 55(3), 418-429.
53) El-Tabl, A.S. (1997). Synthesis and spectral studies on mononuclear copper (II) complexes of isonitrosoacetylacetone ligand, Polish Journal of Chemistry, 71, 1213-1222.
54) El-Tabl, A.S., Abou-Sekkina, M. (1999). Preparation and thermophysical properties of new cobalt (II), nickel (II) and copper (II) complexes, Polish Journal of Chemistry, 73, 1937-1945.
55) El-Tabl, A.S., Abd-El-Wahed, M.M., Refae, R.E.S. (2016). Synthesis, Structural Investigation and Biological Evaluation of New Metal Complexes of 4, 4-((bis (phenylamino) methylene) bis-(azoanylylidene) Bis (hydroxyimino) pentan-2-one Ligand. Journal of Chemistry and Chemical Sciences, 6 (2), 109-126.
56) EL-Tabl, A.S., Wassel, M.A., and Arafa, M.M. (2017). Preparation and investigation of fulvic acid and its metal derivative complexes with application, International Journal of Scientific & Engineering Research, 1663-1679.
57) El-Tabl, A.S., Abd-El-Wahed, M.M., El-Saied, S.A.E.R. (2018). Design, Spectroscopic Charactarization and Antitumor Action of Synthetic Metal Complexes of Novel BenzohydrazideOxime. Journal of Chemistry and Chemical Sciences, 8(8), 1048-1072.
58) El-Tabl, A.S., Abd-El-Wahed, M.M., Mosa1, R.M.H. (2019). Novel metal complexes of dehydroacetic acid hydrazone as platforms for hepatocellular carcinoma therapy , Journal of chemistry and chemical science, 9(4), 128-152.
59) El-Tabl, A.S., Abd-El-Wahed, M.M., El-Henawy, E.M., Abd El-Wahab, O.E., Hashim, S.M.F. (2019).Metal complexes in cancer therapy: Synthesis, spectroscopic characterization and antitumor effect against breast cancer of new dihydroxy phenyl ethylidene amino benzoic acid complexes, International Journal of Scientific and Engineering Research IJSER, 10(3),631-645.
60) El-Tabl, A.S., Abd-El-Wahed, M.M., Ashour, A.M., Abu setta, M.H.H., Hassanin, O.H., Saad, A.A. (2019). Metallo-organic copper(II) complex in nano size as a new smart therapeutic bomb for hepatocellular carcinoma, Journal of Chemistry and Chemical Sciences, 9(1), 33-44.
61) El-Tabl, A.S., Shaban, M.T., Abd El-Wahed, N.M. (2019). Novel Metal Complexes as Antimicrobial Agents, Synthesis and Spectroscopic Characterization, Journal of Chemistry and Chemical Sciences, 9(3), 74-108.
62) El-Tabl, A.S., Abd El-Hamid, I., Abd-El-Wahed, M.M., Ahmed, R.A.S., Ashour, A.M., (2022). Novel nano-metal complexes of modified aspirin as future antimicrobial agents, International Journal of Pharmaceutical Research, Vol 14 (1), 85-111.
63) EL-Boraey, H and EL-Tabl, A.S, (2003), Supramolecular Copper(II) Complexes with Tetradentate Ketoenamine Ligands, polish journal of chemistry, vol 77 (12), 1759-1775.